Energetic Materials Frontiers 1 (2020) 141–156

Contents lists available at ScienceDirect

Energetic Materials Frontiers

journal homepage: www.keaipublishing.com/en/journals/energetic-materials-frontiers

Recent advances on the crystallization engineering of energetic materials

Xue-Xue Zhang [a], Zhi-Jian Yang [b], Fude Nie [b], Qi-Long Yan [a,*]

[a] Science and Technology on Combustion, Internal Flow and Thermostructure Laboratory, Northwestern Polytechnical University, Xi'an, 710072, China
[b] Institution of Chemical Materials, China Academy of Engineering Physics, Mianyang, 621999, China

ARTICLE INFO

Keywords:
Crystallization engineering
Crystal morphology
Crystal defects
Thermal stability
Explosive sensitivity

ABSTRACT

The safety properties and desirable detonation performance of energetic materials (EMs) are mutually exclusive, therefore, various strategies including the coating, doping, crystallization, and co-crystallization, are applied to achieve high-energy insensitive explosives with well-balanced energy and safety level. Among these strategies, the crystallization is the most commonly method owing to its low cost and facile process, through which the tuning of the particle size and morphology, adjust sensitivity of EMs by tailoring the processes conditions. As the control of the crystal particle size is difficult, the ultrasound and electrospray are introduced, and by use of the spray drying or spray-assisted electrospray methods, the spherical RDX, HMX, and CL-20 crystals with less defects is obtained. Moreover, the perfect spherical crystals are gained without agglomeration through employing polymeric additives in the crystallization process. In general, the crystallization with spray drying, electrospray, and ultrasound-assisted solvent/antisolvent are the optimal crystals preparation methods. The nano-crystals with narrow particle size distribution are less sensitive to external stimuli than irregular microcrystals, and defects are associated with hot spots, the safety and energy performance of EMs could be well balanced by crystallization.

1. Introduction

Energetic materials (EMs) are extensively used in civil and military applications, and exists a high demand for their balance of the safety and energy. However, the thermally stable and insensitive explosives usually exhibit poor energy output.[1] At present, the foremost objectives of research in this area are the synthesis of new compounds with high energy content and acceptable safety level[2] and improvement of the energy and safety with the modification of the crystal morphologies of existing explosives.

The preparation of new energetic compounds that exhibit well-balanced safety and energy properties, so-called high-energy insensitive explosives, is usually rather time-consuming.[3,4] For example, the tetranitrocubane (TNC), a promising high-energy insensitive explosive, was hampered by the instability of the cage-like intermediates under the reaction conditions of the synthetic route. 3,3′-Diamino-4,4′-azoxyfurazan (DAAF) with high thermal stability with an onset temperature of 248.8 °C, is extremely insensitive to external stimuli, exhibiting a friction sensitivity of over 360 N and an impact sensitivity (H_{50}) of more than 320 cm at a low density (1.745 g·cm^{-3}), but DAAF cannot be produced on a large scale, in spite the furazans are attractive explosives, and its stacking by the planar geometry enables high densities and plane sliding, which in turn reduces the shear strain caused by impact or shock.[5] Another example is high-performance derivatives of pentazole compounds containing the N_5^- unit but they are only stable under extreme conditions.[6] Obviously, it is challenging that the traditional EMs are replaced by newly synthesized ones.

The crystal modification of EMs was realized by several means including the coating, doping, co-crystallization and crystallization. The coating of high-energy, sensitive explosives such as hexanitrohexaazaisowurtzitane (CL-20) with insensitive ones, for instance triaminotrinitrobenzene (TATB), is vital to reduce the sensitivity of the former.[7] Furthermore, coating of octahydro-1,3,5,7-tetranitro-1,3,5,7-tetrazocine (HMX) with the biomaterial polydopamine (PDA) delivered HMX@PDA with greatly reduced sensitivity.[8] Regard as the doping strategies, PDA, the graphene oxide and carbon nanomaterials such as fullerenes, expanded graphite (EG), carbon nanotubes (CNTs), graphene, and graphene oxide (GO)[9] have been widely used to improve the safety of energetic crystals. For example, we recently reported that the use of a novel hybrid 2D nitrogen-rich and insensitive EM, TAGP, to dope 1,3,5trinitro-1,3,5-triazinane (RDX)[10] and HMX[11] leads to materials with improved energy content and reduced sensitivity. In particular, functionalized carbon nanomaterials with high energy content have been employed to balance the energy and safety of nanoexplosives by coating

* Corresponding author.
E-mail address: qilongyan@nwpu.edu.cn (Q.-L. Yan).

https://doi.org/10.1016/j.enmf.2020.12.004
Received 14 July 2020; Received in revised form 6 December 2020; Accepted 15 December 2020
Available online 23 December 2020

or encapsulation.[12] Furthermore, co-crystallization is known to balance the sensitivity, thermal stability, and energy content of EMs.[13] The cocrystal HMX/TATB has been designed to exhibit reduced sensitivity.[14] However, the co-crystallization with insensitive compounds may reduce the energy content to some extent. These methods may introduce some other materials. In contrast, the crystallization is a physical technique to purify energetic crystals and control their morphology and particle sizes.[15]

Crystallization is widely used because it is cost-effective and does not introduce other materials. Alternatively, high-performance insensitive crystalline EMs are obtained upon purification to improve the crystal morphology and reduce the particle size distribution. And the properties of synthesized EMs could be suitably adjusted by using different crystallization methods. The common crystallization techniques include spray drying, ultrasound-assisted spray, electrospray, rapid expansion of supercritical solutions, and solvent/anti-solvent methods. Typical EMs with different mean particle diameters were obtained by tuning experimental conditions such as temperature, type of solvent, and level of supersaturation.[16] In addition, EMs with a narrow particle size distribution was produced by special techniques such as supercritical fluids.[17] Crystallization enables the access to EMs crystals of refined particle size or morphology and higher purity, including defect-free materials.[18] As such, energetic crystal particulates with a variety of specific desired properties can be fabricated.

Over the past decades, a large number of studies addressing EM crystallization have been conducted. In this review, the common crystallization methods are presented and discussed with a focus on improving the crystal quality of energetic crystals including morphology and particle size control. And the performances of EMs like sensitivity and thermal stability could be enhanced. A comprehensive comparison of the morphology, crystal structures, thermal stability, and sensitivity of energetic crystals prepared by different crystallization methods was drawn. As a general trend, the insensitive energetic crystals of higher purity and containing fewer defects are obtained *via* crystallization, which reduces the hot spots ultimately improving the safety.

2. Crystallization strategies for energetic compounds

Crystallization is a natural process through which materials solidify from liquids or precipitate from liquid or gaseous solutions.[19] This process consists of the assembly of atoms or molecules in highly ordered structures, termed crystals, and can be triggered by changes in the physical or chemical environment, such as temperature or pH, respectively. The crystallization process usually involves nucleation and crystal growth.[20] As for the EMs, the spray crystallization and solvent/antisolvent crystallization are common strategies to improve the energetic crystals quality. In this review, the effects of crystallization on the crystal structure and performance of RDX, HMX, and CL-20, which are selected as representative EMs, are discussed with a focus on the influence of the crystallization parameters on the crystal defects, sensitivity, and thermal stability.

2.1. Crystallization by spray

2.1.1. Basic mechanisms

Spray crystallization is a single-step method that produces various mono- or multicomponent functional micro- and nanoparticles. The energetic crystals with uniform particle size and nearly spherical regular particle shape could be obtained by this method.[21] To avoid chemical decomposition during the spray drying crystallization process, the boiling temperature of the solvents should be as low as possible considering the sufficient solubility.[22] Spray crystallization is highly suited for the continuous production of dry crystals. There are three steps involved in spray drying. Firstly, the liquid feed is atomized into small droplets. Then, these spray droplets are mixed with the heated air flow to evaporate the solvent and the dried powder are left. The powder is collected in the last step. In this case, less dense samples with smaller average particle sizes and narrower size distributions are obtained.

2.1.2. Crystallization by spray drying

The obtained crystals could be defect-free or with hollows upon design, depending on the operating conditions. The latter case results from solute precipitation on the surface of a droplet that is not oversaturated in its center.[23] It has been found that the spray pressure, temperature, feeding rate and solution concentration have a significant effect on the particle size. For instance, the large droplets with low concentration would evaporate quickly without agglomeration to form nanoparticles.[24] A typical EM application of spray drying crystallization is the large-scale production of HMX[25] with a mean particle size of 400 nm.

Although spray drying is a promising way to produce large scale EMs, it suffers from inherent limitations. The major disadvantage is high temperature to evaporate the solvent, difficulty controlling particle size and particle size distribution. In order to solve these problems, other techniques have been introduced like electrospray and Rapid Expansion of Supercritical Solutions (RESS).

Electrospray crystallization is a further advanced method to produce nano- and submicron-sized energetic crystals with less aggregation[26] and controlled crystal morphology. However, the low efficiency of this technique limits its use to gram-scale.[27] In electrospray crystallization (Fig. 1a), a mist of ultrafine solution droplets is generated. Subsequent solvent evaporation leads to crystallization of submicron-sized crystals.[28] For example, hollow spherical RDX crystals were obtained at relatively small nozzle diameters and relatively low potential differences, whereas larger nozzles and higher potential differences approaching a continuous jet delivered products with larger average particle sizes. The RDX nanoparticles (500 nm) with a narrow particle size distribution obtained by this method[29] are less sensitive due to fewer inclusions and crystal defects.

The RESS process is commonly used in the food, cosmetics, and pharmaceutical industries to produce fine powders[30] in two steps. After dissolution of the solid substance in a supercritical fluid (SCF), particle formation occurs due to supersaturation.[31] This technique also enables fabrication of EM nanocrystals, as shown in Fig. 1b. Following dissolution

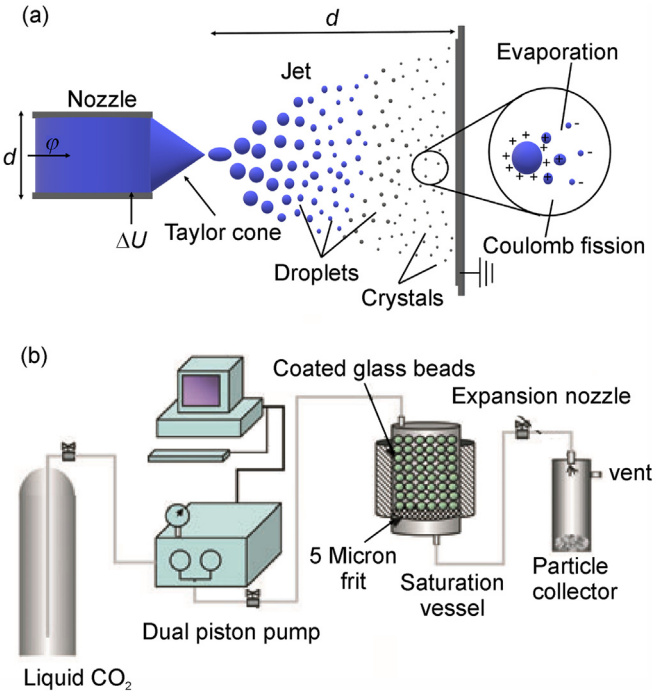

Fig. 1. (a), Electrospray crystallization process diagram.[28] (b), Schematic representation of the RESS setup.[34]

of the EM in supercritical carbon dioxide, rapid expansion of the supercritical solution in the precipitator causes a pressure and temperature decrease that favors the formation of small crystals with a narrow particle size distribution.[32] Hence, this technique is well-suited for the production of low-defect submicron-sized particles with a narrow size distribution.[33,34]

Submicron-sized RDX particles with granular or spherical morphology have been produced by the RESS method in small scale.[35] The significant effect of the extraction temperature, extraction pressure, and size of the nozzle orifice on the morphology and particle size of the RDX crystals were studied using compressed liquid dimethyl ether (DME) as a solvent. While higher extraction temperatures and smaller nozzle sizes favor formation of smaller RDX particles, a higher extraction pressure leads to larger particles. In average, the precipitated RDX particles ranged from 0.36 to 2.48 μm. However, the enthalpy of the exothermic decomposition of the obtained RDX increased considerably from 381.5 to 714.4 $J{\cdot}g^{-1}$. In a similar approach, supercritical dimethylformamide (DMF) was used to dissolve raw RDX while CO_2 was used as an antisolvent which allowed the preparation of a fine RDX powder by RESS in a high-pressure crystallization vessel.[36] However, the gravest disadvantage of the RESS process is the high CO_2 consumption. For example, the highest RDX production capacity of approximately 5–6 $g{\cdot}h^{-1}$ was achieved at a CO_2 flow rate of 35 $kg{\cdot}h^{-1}$[34] Thus, the large-scale production of nano-EMs by this method is unattractive because of the high cost of CO_2 and the potential risks posed by the high working pressure.

2.2. Crystallization by solvent/antisolvent

2.2.1. Basic principles

Crystallization by solvent/antisolvent is widely used in purifying energetic crystals and improving the crystal quality of it because of low cost, safety, and convenience.[37] In this process, supersaturation is achieved by employing antisolvent which is usually added to a (concentrated) solution.[38] The antisolvent and the solvent are typically well-miscible, while the crystallizing product has a lower solubility in the antisolvent.

2.2.2. Solvent/antisolvent technique

The lower sensitivity of explosives, such as HMX and RDX, obtained by the solvent/antisolvent process is possibly due to the reduction in the number of internal defects and impurities. Crystallization generates nano-TATB crystals with less surface defects.[39,40]

However, the access to fine crystals with uniform morphology and particle size is problematic for most EMs using solvent/antisolvent method. The crystals produced by this method could be nonuniform because the crystals morphology and particle size are highly influenced by the experiment conditions like stirring rate, room temperature and even the dropping speed of antisolvent. Thus, the properties of produced crystals could be different in the different part of container. In addition, it is extremely difficult to synthesis nanoparticles with a narrow size distribution. For this reason, a lot of technologies like spray and ultrasound have been introduced to obtain uniformed crystals.

Ultrasound have a positive effect on the nucleation process as well as control crystallization which gives rise to an acoustic cavitation in liquid media and moreover influences the crystal nucleation and growth.[41] Therefore, some EMs like fine CL-20 particles with desired morphology could be produced using ultrasound-assisted precipitation method.[42] The CL-20 precipitates when the antisolvent is added in the presence of ultrasound which has greatly reduced the agglomeration of obtained CL-20.

The introduction of the spray technique to solvent/antisolvent crystallization has facilitated the control over the crystal morphology, purity, crystal imperfections and particle size to achieve the desired insensitivity levels.[43] Submicron-sized HMX samples with fewer crystal defects were produced *via* the spraying technique in acetone with water as the antisolvent. In addition, the particle size and crystal morphology of HMX can be modulated by adding a surfactant. For example, addition of isopropyl alcohol to the antisolvent leads to a decrease in the droplet stability which is accompanied by a decline in the particle size. Regarding safety and production aspects, the spherical shape is the most desirable morphology of EM crystals. For instance, the approximately aggregate spherical particles keto-RDX (2-oxo-1,3,5-trinitro-1,3,5-triazacyclohexane) could be made by spraying crystallization method[44] with a high density of 1.93 $g{\cdot}cm^{-3}$[45]

In contrast to dropping techniques, the spray process not only atomizes the solution but also increases the mass and heat transfer rate of the atomized droplet.[46] Hence, the introduction of ultrasound and spray techniques together to solvent/antisolvent EM crystallization processes simplifies the control over the point of nucleation and number of nuclei.[47] Regarding 2,2′,4,4′,6,6′-hexanitrostilbene (HNS), the shape changed from long needle-like crystals to elongated rods and polyhedral-shaped ones with negligible defects after crystallization by the ultrasound and spray-assisted technique solvent/antisolvent method (Fig. 2).[48] In this process, HNS was dissolved in DMF and the solution was forced through the inlets of the nozzle at the required high pressure and flow rate, thereby forming a spray of fine droplets upon exiting the nozzle. The resulting atomized solution underwent micromixing with the antisolvent in a flask that was maintained at the required temperature inside of an ultrasonication tub (45 kHz). Due to the high degree of supersaturation, micromixing in the flask led to a very rapid dispersion and high nucleation rate, ultimately delivering fine HNS explosive crystals with a narrow particle size distribution.

2.3. Other crystallization methods

2.3.1. Reaction crystallization

In reaction crystallization, the solute's solubility is reduced through the addition of a reactant to form a different substance or pH adjustment to trigger pH-shift crystallization.[49] In these processes, the formation of the solid phase results from a chemical reaction between the components originally present in the feed streams, for instance A (aq) + B (aq)→AB (s). The pH-shift crystallization usually exploits pH-dependent changes in the chemical state or charge of ionic species. Well-known examples of ions that exhibit pH-dependent states are carbonate and phosphate. Typically, this method relies on acid–base reactions, very fast processes that can be considerably exothermic, especially at high reactant concentrations. Therefore, reactive crystallization is mostly employed to crystallize ionic crystals.

Fractional crystallization is a process in which successive crystallization steps are performed to increase the product's purity and/or the yield of the process in an industrial production setting.[50] In this process, the crystals formed in the first crystallization step are separated from the mother liquor using a filter, centrifuge, or wash column, remolten, and used as feed in the second crystallization step, which is conducted at a higher temperature due to the higher purity of the feed.[51]

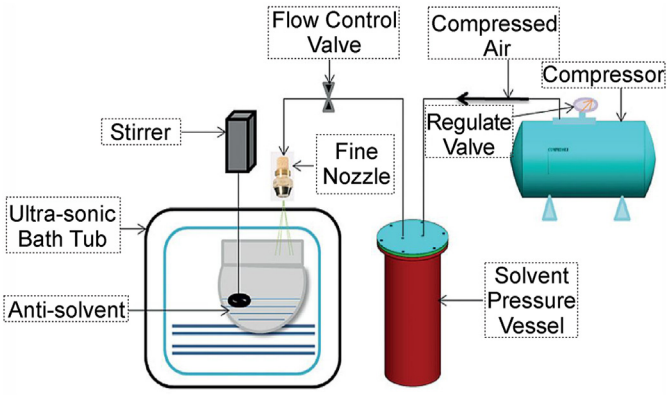

Fig. 2. Schematic of the ultrasound and spray-assisted solvent/antisolvent crystallization.[48]

In principle, fractional crystallization encompasses crystallization from both solution and melt, whereas in practice it is more commonly used for the latter. In turn, the fractional melt crystallization method is an attractive alternative to distillation for the separation of organic mixtures.[52] Although distillation is by far the most frequently employed separation process in the chemical industry, it has distinct disadvantages such as thermal degradation of the product, high energy consumption, and poor performance in the case of azeotropes. Regarding explosives, control of the morphology is predominantly achieved by the evaporative and precipitation-crystallization methods.2.3.2 Sol-gel crystallization.

In the sol-gel method, the reactants initially form nanosized primary particles, which are suspended in a solution termed sol. As these particles continue to cross-link, the solution viscosity increases until a three-dimensional solid network is produced. The unreacted liquid that remains in the network pores is termed gel.[53] The sol–gel technique is used for the preparation of EMs (explosives, propellants, and pyrotechnics) with improved homogeneity. For example, RDX crystals with few defects randomly dispersed in a silica aerogel[54] were obtained by solution crystallization, in which the energetic material crystallized within the pores of a sol–gel-derived solid. To this end, the solvent used to dissolve the explosives is compatible with the reactants and allows control over the density of the resulting gel. Subsequently, gel mending enables the uniform loading of the explosive powder in the gel. This process results in a significant improvement in the material's safety performance (impact sensitivity and thermal stability). In addition, the sol–gel method is used to synchronize the coagulation process and the crystallization of explosives in the sol, thus delivering ultrafine small explosive particles in-situ.[55] Moreover, nano-RDX/RF films prepared by this method feature adjustable RDX content and energy output characteristics. Therefore, these materials are potentially useful in the development of microminiature pyrotechnic products. Additionally, sol–gel crystallization was used to synthesize a porous monolithic metal–organic framework (MOF),[56] with an at least 130% greater hardness than that of its conventional MOF counterparts.

2.3.2. Green mechanical demulsification crystallization

The majority of the discussed crystallization methods require large amounts of solvent, which is environmentally harmful. In contrast, green mechanical demulsification crystallization is among the eco-friendly methods to prepare EMs crystals with regular morphology, smooth surface, and narrow particle size distribution. For example, fine RDX crystals with few defects were obtained by mechanical demulsification of a well-mixed RDX, purified water, and composite emulsifier mixture.[57] Further, the H_{50} of RDX improved from 24.34 to 45.78 cm upon mechanical demulsification, whereas this value increased to 33.21 cm when RDX was subjected to the solvent/antisolvent technique.

2.3.3. Comments and summary

Nearly all crystallization methods lead to the improvement of crystal quality such as the reduction in the internal crystal defects, crystal surface defects and particle size distribution. While the solvent/antisolvent technique is among the most cost-effective, single-step methods that deliver defect-free crystals. Its major disadvantage is the high solvent consumption and the broad particle size distributions. Further, the crystal quality is influenced by parameters such as temperature, concentration, solvent, and string speed.

The strengths and drawbacks of various crystallization methods are presented in Table 1. However, inherent drawbacks of these techniques include limited choice of solvents, hazards associated with friction and impact, undesired polymorph transformation, difficult control over the particle size, and upscaling restrictions, among others.

The solvent/antisolvent technique, particularly for fine HMX, was reviewed in detail due to its high relevance for in-house developmental activities. A limitation of the mentioned above methods for nano- or microexplosive production is severe agglomeration.[58] Much research has addressed this issue by examining surfactant additives, ultrasound technology, and supercritical fluid drying. In this context, ultrasound- and spray-assisted solvent/antisolvent crystallization presents a solution to this problem. Finally, the recently popularized RESS method features straightforward particle size and size distribution control, but has limited applicability in industrial manufacturing and safety processing.

Table 1
Advantages and disadvantages of several crystallization methods.

Method	Advantages	Disadvantages
Spray crystallization		
Solvent evaporative crystallization	Efficiency, low cost, narrow particle size distribution	Agglomeration, high temperature, large particle size distribution
Spray crystallization	Low cost, suitable for large scale production	High temperature, high solvent consumption
Melting spray crystallization	Low cost, suitable for large scale production	Restricted to low-melting crystals
Ultrasound spray crystallization	Suitable for large scale production, narrow particle size distribution, uniform crystal morphology	Risk of increase in crystal defects by the required external mechanical force
Electrospray crystallization	Less agglomeration, narrow particle size distribution, uniform crystal morphology	High cost, limited to gram-scale
Crystallization by Rapid Expansion of Supercritical Solutions (RESS)	Less agglomeration, narrow particle size distribution, accurate particle size and morphology control	High antisolvent consumption, high cost, operationally complex
Solvent/antisolvent crystallization (SA)		
Solvent/antisolvent crystallization (SA)	Low cost, suitable for large scale production	Limited control over crystal shape and size, high solvent consumption
Ultrasound-assisted solvent/antisolvent crystallization (UASA)	Less agglomeration, narrow particle size distribution, uniform crystal morphology	High solvent consumption
Spray-assisted solvent/antisolvent crystallization (SASA)	Less agglomeration, narrow particle size distribution, uniform crystal morphology	High solvent consumption
Ultrasound- and spray-assisted solvent/antisolvent crystallization (USASA)	Less agglomeration, narrow particle size distribution, uniform crystal morphology	High solvent consumption
Other methods		
Sol–gel crystallization	uniform crystal morphology, straightforward particle size and morphology control	High cost
Green mechanical demulsification crystallization	Environmentally friendly, suitable for large scale production	Difficult crystal morphology control

3. Strategies for energetic crystal quality improvement

The crystal quality of energetic materials such as particle size, crystal surface morphology and crystal internal defects are important factors affecting the safety performance, mechanical properties and processing performance of explosives.[59,60] Most importantly, crystal quality can be improved through crystallization process. The crystal quality is not only influenced by its own crystal defects and particle size distribution, but also by crystallization methods and external crystallization parameters such as solvent, antisolvent, and temperature.[61–63] High-quality energetic crystals with significantly improved overall performance can be obtained through different crystallization methods.

3.1. Crystal morphology control

The crystal morphology is influenced by the internal crystal defects like voids, bubbles, cracks, impurities and surface defects such as sharp

features. Crystallization is a common strategy to reduce the crystal defects.[64] However, the results could be different using different crystallization methods. As shown in Fig. 3, the raw RDX (Fig. 6a),[36] HMX (Fig. 6b),[65] and CL-20 (Fig. 6c)[66] samples feature irregularly shaped crystals with rough surface. As explosives with more crystal defects are more sensitive than those with fewer defects, the aim of crystallization engineering is to produce EM crystals with fewer inner voids or defects, smooth surface, and a regular block or spherical shape. Several attempts had been made to improve the crystals' quality.

Conventional nitramine explosives with large crystal defects or void morphology fail to satisfy the requirements for military development because they are important hot spot triggers.[67] The sensitivity can be decreased by avoiding hot spot generation and propagation such as reducing crystal defects, producing of spherical crystals, or decreasing in the particle size.[68] Fig. 6 shows that crystallized explosives have fewer crystal defects.

The crystals obtained by solvent/antisolvent method (dropping solvent to antisolvent or dropping antisolvent to solvent) are easily aggregate. However, drop-to-drop (DTD) mixing of the solvent and antisolvent yielded SM-sized particles continuously in flow.[69] As shown in Fig. 3b, well-dispersed nearly spherical RDX crystals obtained *via* drop-to-drop solvent/antisolvent crystallization have smooth surfaces and few crystal defects. On the other hand, a novel spray drying assisted self-assembly (SDAS) technology is also a promising method to produce defect free nano explosives. For instance, the r-RDX crystals (Fig. 3c) with fewer defects and a smooth surface at a narrow particle size distribution could be obtained by this method.[37] During this crystallization process, PVA plays an important role in discharging acetone out of the drying chamber. For one thing, it could effectively limit the growth of the crystal planes of RDX crystals, and for another, it could actively prevent agglomeration during nucleation of RDX crystals. In addition, introducing self-assembly technology to spray drying may lead to improvement in sensitivity and thermal stability. As for the r-RDX, the H_{50} has risen from 25.6 to 48.3 cm and the friction sensitivity has decreased from 92 to 62%.

In the same with crystallized RDX (Fig. 3b), the obtained HMX crystals by DTD method (Fig. 3e) have defect free spherical surface while the crystallized HMX crystals using RESS method are prismatic shape with smooth surface and obvious edges.[68] Among recently used explosives, CL-20 has the largest detonation velocity. However, its high sensitivity to impact, friction, shock wave, and electrostatic spark stimuli strongly limit its application range in weapons. The spherical r-CL-20 crystals (Fig. 3h) obtained *via* the ultrasonic spray-assisted electrostatic adsorption (USEA) method have fewer defects.[70] Furthermore, crystallized CL-20 (Fig. 3i) features polyhedral and nearly spherical crystals with negligible defects or cracks.[65] Thus, reducing crystal defects is a promising strategy toward sensitivity reduction while maintaining the energy performance. Overall, the crystallization methods like solvent/antisolvent or spray drying method could reduce the crystal defects to some extent, introducing some external force like ultrasound or adding some surfactant could largely avoid aggregation and producing crystals with smooth surface.[71]

Except for the crystallization strategies we mentioned above have different influence of crystal properties, the experiment conditions such as solvent, temperature, agitating speed, and degree of supersaturation also affect the morphology and crystal structure.[72] Take 3,5dinitropyrazine-2,6-diamine-1-oxide (LLM-105) as an example, LLM-105 forms rough surface when it is crystallized form ethyl acetate (Fig. 4a) while smooth and X-shaped crystals are crystallized from water (Fig. 4e). Furthermore, rod-shaped crystals are obtained by crystallization from nitromethane (Fig. 4f). Preparing the spherical crystals of organic explosive molecules is a promising strategy to reduce the crystal defects. However, it is quite difficult to crystallize EMs crystals which contain strong intra- and intermolecular hydrogen bonds, such as LLM-105, spherical LLM-105 crystals are obtained by advanced strategies in which polymeric additives prompted modification of the crystal habit.[46] In the absence of PVP as a polymeric additive, crystallization delivers X-shaped LLM-105 crystals with considerable amount of defects (Fig. 4a).[47] PVP leads to a significant reduction in the aspect ratio, thus forming crystalline LLM-105 nanofibers. Therefore, smooth, defect-free, spherical LLM-105 crystals are obtained with an average particle size of 78.0 μm and a narrow size distribution (Fig. 4d).

The crystal growth could be altered by crystallization process. Dendritic RDX potentially exhibits particular properties and likely represents a new modification of single composite explosives.[75] The in-situ observation technique was used to study the mechanism of crystal growth. Following addition of surfactant 1631 to a RDX solution in cyclohexanone (CHN), in-situ imaging of the dendritic crystal growth is presented

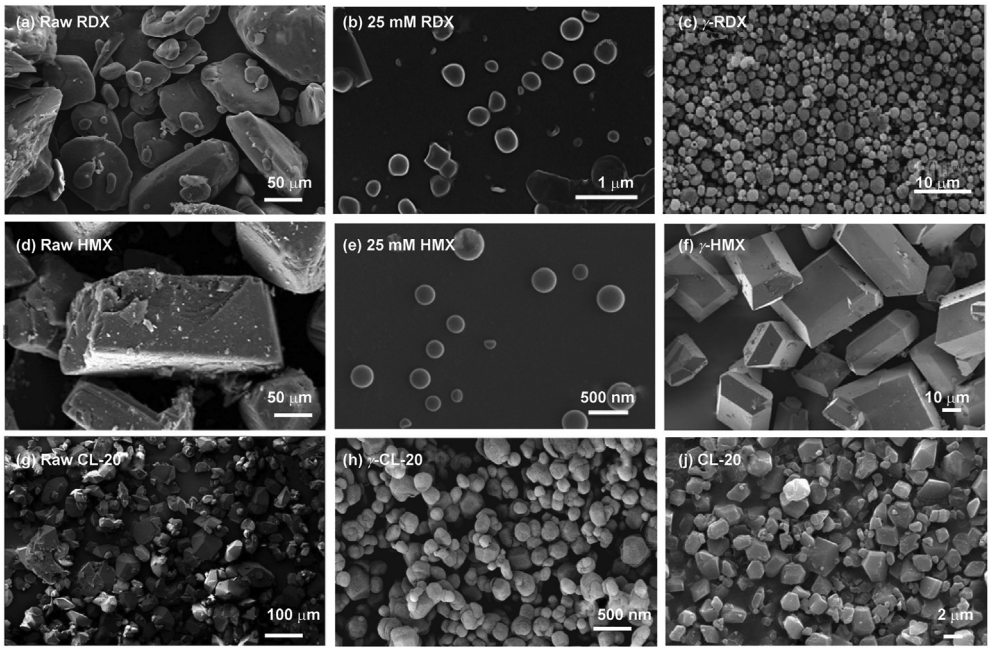

Fig. 3. SEM images of different EMs. (a) Raw RDX,[36] (b) RDX and (e) HMX after solvent/antisolvent crystallization,[69] (c) RDX after SDAS,[37](d) raw HMX,[65] (f) HMX after the RESS process,[68] (g) raw CL-20,[66](h) CL-20 after USEA,[70] (i) CL-20 after ultrasound- and spray-assisted crystallization.[65]

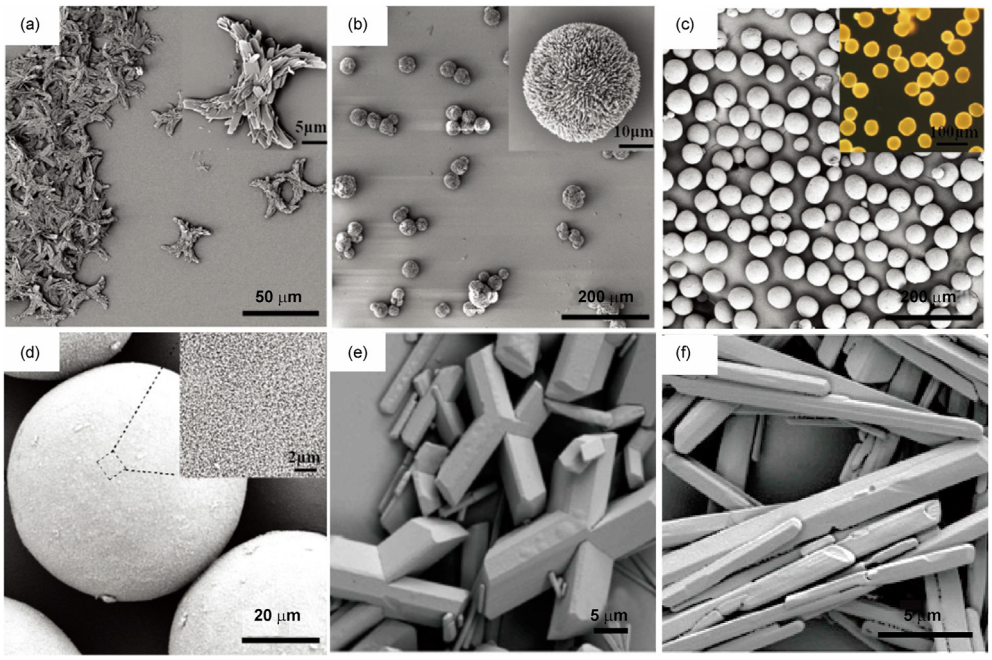

Fig. 4. SEM images of LLM-105 crystallized using: (a) ethyl acetate,[73] (b) diluted PVP in ethyl acetate,[73] (c) and (d) concentrated PVP in ethyl acetate,[73] (e) water,[74] and (f) nitromethane[74] as the antisolvent.

in Fig. 5. Images a–e show the nucleation and early stages of the growth process of typical boundary dendrites, revealing that the crystal grows along the negative concentration gradient. Fig. 5f–j display the progress of the growth process, in which the preferential growth of the "fold'' occurred nearly vertical to the solution boundary layer.

The crystal morphology also can be altered by crystallization, as shown in Fig. 6a, HMX crystals precipitated from DMSO and GBL have a truncated octahedron shape. In contrast, crystals obtained from DMF have a hexagonal plate shape, whereas those prepared from acetonitrile (ACN) and CHN are truncated octahedron and the plate form of the truncated octahedron shape, respectively. To investigate the influence of crystallization on HMX crystal forms, the HMX with different morphologies were conducted by FTIR (Fig. 6b). The absence of peaks between 700 and 740 cm^{-1} in the spectrum of β-HMX[76] confirmed that raw HMX and HMX precipitated from DMSO and GBL have the same phase. In contrast, the peaks at 713 and 739 cm^{-1} observed for crystals obtained from DMF are characteristic of δ-HMX. Furthermore, the γ-phase was identified for the HMX particles precipitated from ACN and CHN by the peaks at 709 and 732 cm^{-1}. It was reported that the low-density γ-HMX could also transform into β-HMX upon precipitation during the solvent/antisolvent process.[77]

`As the same with HMX, the crystal forms of RDX and CL-20 were affected by crystallization process.[78] The different crystal forms of RDX, HMX, and CL-20 are shown in Fig. 7. Regarding RDX, the thermodynamically stable α-phase is formed directly during crystallization. As for CL-20, the α-form is a hydrate at ambient conditions, whereas the ξ-form only exists at high pressures.[79] The ε-CL-20 has the highest density (2.04 $g{\cdot}cm^{-3}$) and a detonation velocity of 9660 $m{\cdot}s^{-1}$[80,81] Therefore, the main purpose of CL-20 crystal engineering of is to produce the ε-form while avoiding crystal transformation to other forms,[82] which occurs at low temperatures, including room temperature.[83] Moreover, the morphology of CL-20 transforms from needle-to diamond-shaped crystals in solution, which indicates the polymorphic transformation from the β-to the ε-form.[84]

3.2. Crystal particle size modulation

The particle size and particle size distribution play a decisive role in the EM performance. A reduction of the particle size of

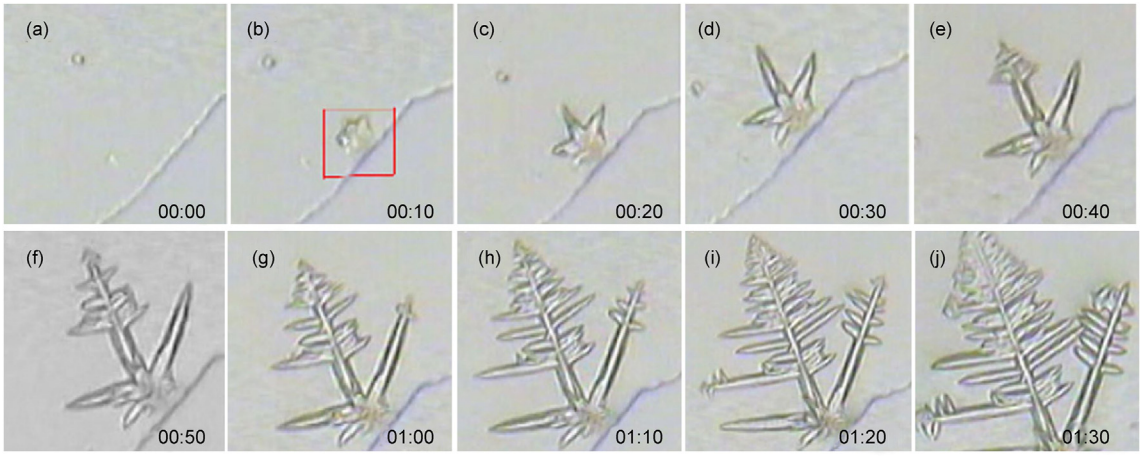

Fig. 5. [75] Typical growth process of RDX dendrite at the solution film boundary of the cyclohexanone solution with surfactant 1631 added.

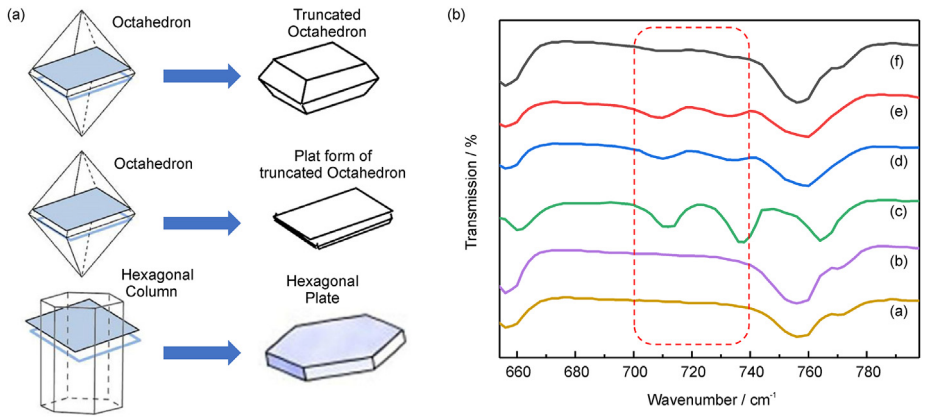

Fig. 6. (a), Crystal structures of HMX particles crystallized from various solvents by the GAS process[65]; (b), FTIR spectra of (a) raw HMX and HMX crystallized *via* the GAS process from (b) DMSO, (c) DMF, (d) ACN, (e) CHN, and (f) GBL.[65]

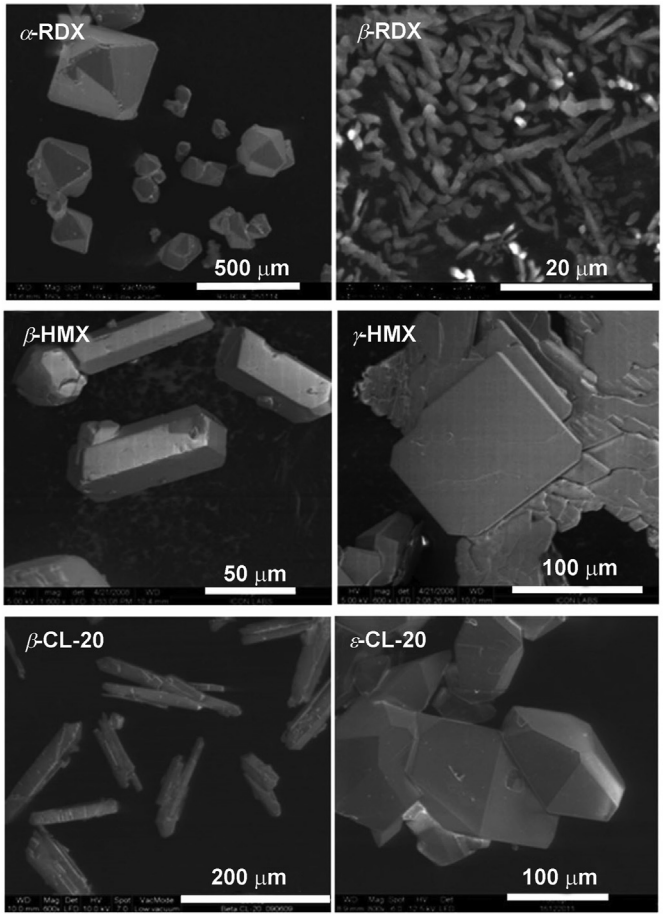

Fig. 7. SEM images and Raman spectra of RDX, HMX and CL-20 polymorphs with different crystal forms.[78]

conventional EMs to micro- or nanometer scale is associated with higher burning and decomposition rates and lower impact sensitivity.[85] The larger surface area of nanoexplosives leads to an improved heat transfer ability, which in turn reduces their sensitivity to the formation of hot spots due to impact or friction. In particular, the friction sensitivity of RDX decreases linearly as the particle size drops from 154 to 10 μm.[86] Additionally, the sensitivity of nitramine explosives, including HMX, is directly affected by its particle size and distribution.[87] In this section, we present numerous methods used to produce fine EM powders.

The particle size of EMs also is effect by the crystallization process. Raw RDX crystals (Fig. 8a) have irregular shapes and their particle size distribution is wide. As shown in Fig. 8, RDX crystals with less crystal defects and desirable particle size were prepared by the RESS method and by ultrasound spray crystallization. For example, RESS using DMF and CO_2 as the antisolvent delivered small and irregularly shaped RDX crystals (Fig. 8b)[30] with much lower density (1.5 g·cm^{-3}) and the particle size is in the broad range of 1–20 μm. Taking CO_2 as an antisolvent, the crystallized RDX crystals (Fig. 8d) by RESS method are spherical with a particle size of 110 nm.[88] Furthermore, the ultrasound spray method is a further promising strategy to produce spherical EMs crystals. It was reported that the increase in the solution concentration led to formation of large spherical RDX crystals.[89] In contrast, the particle size of microcrystalline RDX (Fig. 8c) obtained at 0.5 wt% RDX solution in acetone was 0.8 μm, whereas larger crystals (2.6 μm) were formed from a 4.0 wt% RDX solution in acetone.

As shown in Fig. 8e, raw HMX is polyhedral with a broad particle size distribution ranging from 50 to 150 μm. After crystallization by ultrasound and spray-assisted method, nano-HMX has a narrow particle size distribution of 40–130 nm and an average diameter of 81.4 nm (Fig. 8f). However, aggregation occurred due to the high surface energy. HMX crystals obtained by the RESS method (Fig. 8g) are smooth and 19.9 μm large in average. While in the liquid, nano-HMX is well dispersed. However, drying from different solvents leads to much larger particles with broader size distributions. Thus, the aggregation of nanoexplosives remains an issue that should be addressed. Ultrasound can provide the phase isolation of microdroplet reactors.[91] Fine non-aggregated micro-HMX crystals with a mean particle size of approximately 4 μm (Fig. 8h) were successfully produced by ultrasound-assisted spray crystallization.[92] The morphology of the ultrafine HMX crystals is mostly ellipsoidal with narrow particle distribution.

The production of nanoparticles with narrow size distribution is unrealistic by the solvent/antisolvent crystallization process because crystals formed from concentrated solutions tend to grow during particle processing. Hence, crystals with a wider particle size range are obtained rather than nano- or micro-sized particles. The mean particle size of CL-20 was largely reduced by several crystallization techniques. At the same time, the crystal form (α- and ε-CL-20) could be controlled by the conditions of the pressurized nozzle-based solvent/antisolvent crystallization.[66] The obtained α-CL-20 (Fig. 8j) features polyhedral and nearly spherical geometry with an average particle size of 3.64 μm. By tuning crystallization conditions such as solvent, antisolvent, stirring speed, pressure, and temperature, ε-CL-20 (Fig. 8k) was produced with an average particle size of 2.27 μm. Importantly, these are nearly round with few surface defects. Thus, the material is more insensitive to external stimuli. Using the USEA method, fine spherical CL-20 crystals with soft agglomeration were obtained (Fig. 8i)[70] in a narrow size distribution

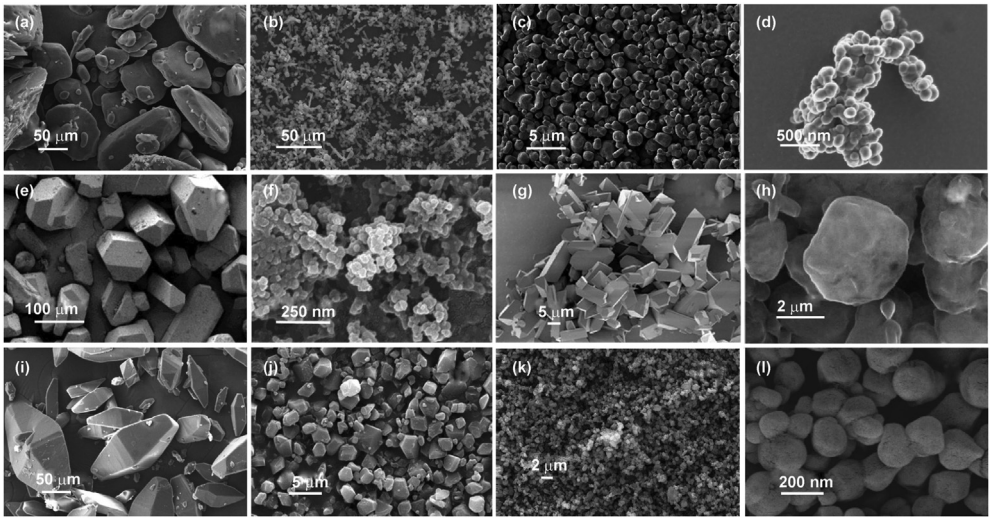

Fig. 8. SEM images of (a) raw RDX,[36] (b,d) RDX after crystallization by the RESS method,[36,88] (c) RDX after ultrasound spray crystallization,[89] (e) raw HMX,[90] (f) crystallized HMX by ultrasound and spray-assisted crystallization method[90], (g) crystallized HMX by RESS method,[65] (h) crystallized HMX by ultrasound spray method,[81] (i) raw CL-20,[70] (j,k) crystallized CL-10 by ultrasound and spray-assisted method[66] and (e) crystallized CL-20 by USEA method.[70]

with an average particle size of approximately 270 nm. In contrast to the preparation of nano-CL-20 by the drowning-out crystallization technique, the USEA method allowed crystallization without antisolvents. Thus, nano-CL-20 was continuously obtained. Furthermore, this technique is suitable for the large-scale preparation of other nanoexplosives.

Crystallization parameters such as the solvent and drying conditions play an important role in the shape, particle size, and particle size distribution of crystalline HMX.[93] As shown in Fig. 9a, industrial HMX consists of angularly polyhedral, heterogeneous particles with average size of 120.36 μm and a wide size distribution. Crystallization using a bi-directional rotation mill led to a sharp decrease in the HMX particle size, which was strongly dependent on the employed solvent. The use of ethyl acetate in the milling process led to an average particle size of 1.9 μm, whereas the diameter of the particles ranged from 1 to 5 μm (Fig. 9b). Furthermore, the use of ethanol delivered particles of under 3 μm with an average size of 1.66 μm (Fig. 9c). In addition, HMX powders obtained using isopropyl alcohol and water had an average particle size of 1.46 and 1.42 μm, respectively (Fig. 9d and e), whereas drying in the miscible liquid led to an average particle size of 1.18 μm with all particles below 2 μm (Fig. 9f). Moreover, the drying method influenced the morphology and particle size of the obtained HMX. When the liquid is removed by evaporation (Fig. 9g), an average particle size of 1.49 μm with a broad size distribution of up to 10 μm was observed. In this case, the nanoparticles tend to agglomerate and grow, thereby overcoming the huge specific surface energy. As the extent of agglomeration is greater for poor dispersions, supercritical and free drying methods are employed to produce nano-HMX with narrow particle size distribution in the range of 200–300 and 100–200 nm, respectively.

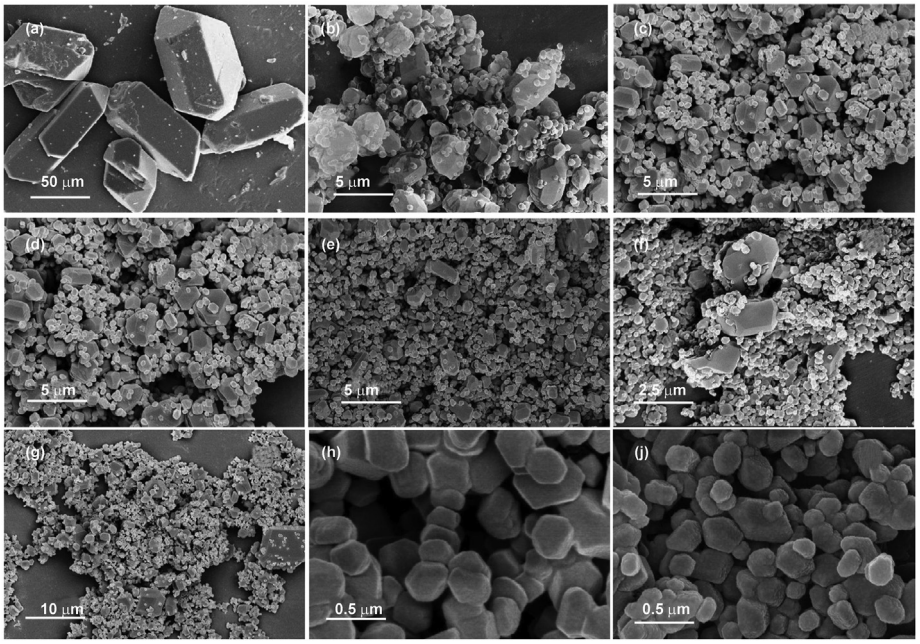

Fig. 9. The SEM images[93] of raw HMX(a) and crystallized HMX under different conditions (ethyl acetate, b; isopropanol, c; alcohol, d; water, e; miscible liquid, f; vacuum drying at 70 °C, g; supercritical drying, h and freeze drying, j).

4. Performances of the high quality energetic crystals

4.1. Sensitivity performance of crystallized crystals

In recent years, much research was conducted to reduce the sensitivity and improve the thermal stability of EMs.[94,95] In this context, it has been reported that the sensitivity of EMs could be reduced through the decrease in the crystal defects and particle size by several crystallization method.[96] Smaller crystals that contain less inclusions and defects are of a higher crystal quality.[97,98] Thus, the application of nano- or micrometer-sized EM crystals with a considerably lower defect content has the potential to further decrease the sensitiveness of the explosives. Recent advances in this area are summarized in Tables 2 and 3 and Fig. 10.

As shown in Fig. 10a, the impact sensitivity of RDX could be reduced by crystallization and the different crystallization methods have different influences on its impact sensitivity. For instance, the impact energies of crystallized RDX by spray drying (r-RDX), spray assisted solvent/antisolvent (micro-K6), electrospray (α_e-RDX) are 17.1 J, 12.3 J and 10 J, respectively. It can be find in Fig. 10a that coating is a promising strategy to reduce the sensitivity as the e-RDX obtained with an Estane coating has the highest impact energy at 37.6 J. Crystallized RDX from the RDX/Estane solution leads to particles coated with the binder, which prevents friction between the explosive particles and acts as a shock absorber or diverter under mechanical stimuli, thereby reducing the probability of hot spot formation However, the introduction of Estane can reduce the energy content of RDX.

The spray-assisted solvent/antisolvent method is an effective, continuous, and safe procedure for the preparation of ultrafine nano-K-6 crystals.[44] The impact sensitivity values of micro- and nano-K-6 are 25 and 30 cm, respectively, indicating that small RDX particles are less sensitive than larger ones. Further, the α_e- and α_p-RDX samples were obtained by electrospray and plasma-assisted crystallization, respectively.[104] It can be found that the friction sensitivity is reduced largely even surpassed the range of friction sensitivity machine (>360 N) both by electrospray and plasma-assisted crystallization. However, the impact sensitivity of α_e- and α_p-RDX are not declined much and the impact sensitivity of RDX obtained *via* plasma-assisted crystallization is the same as that of the conventional RDX. Compared with raw RDX, crystallized RDX consists of smaller, smoother particles with less crystal defects and narrow particle size distribution. These properties prevent the formation of hot spots under mechanical stimuli, leading to a reduced sensitivity. Overall, the spray crystallization or spray assisted solvent/antisolvent crystallization are more suitable for RDX crystals to reduce the impact sensitivity.

The sensitivity of HMX could also be reduced by crystallization and the impact sensitivity varies with the crystallization methods and crystallization conditions. The crystal morphology and particle size of crystallized EMs crystals by some crystallization methods could be different, it will have an influence on the sensitivity. For example, the micrometer-sized spherical γ_s-HMX crystals produced by electrospray require an impact energy of 10 J for ignition, whereas 30 J are required to ignite by toroidal γ_d-HMX, in contrast to the 5 J impact sensitivity of conventional β-HMX.[104] Moreover, the HMX-1, HMX-2 and HMX-3 are obtained *via* solvent/antisolvent method with the particle size of 380–580 nm, 1–10 μm and 10–15 μm, respectively. However, the impact sensitivity of HMX-1, HMX-2 and HMX-3 are 25.6, 8.5 and 7.5 J, respectively. In contrast, the friction sensitivity is independent from the particle size. The main cause of hot spot formation during impact is the adiabatic compression of the cavities in the explosive. Upon friction, the hot spots of explosives mainly result from friction, viscous, or plastic flow. Hence, crystals featuring smooth surfaces are less sensitive to friction stimuli. Micro- and nano-HMX were obtained by the ball milling method and subsequently dried by ordinary (O-HMX) and freeze drying (F-HMX), respectively.[86] As the latter consists of smaller crystals with less defects, it is less sensitive to impact and shock stimuli.

It was found that the sensitivity of HMX crystals is highly influenced by the particle size and morphology. Spherical s-HMX is the stable sample with an impact sensitivity of 26.5 J. In contrast, the facile formation of hot spots on the surface of needle-shaped n-HMX is reflected in its sensitivity to external stimuli (8.4 J impact sensitivity). In addition,

Table 2
Performance of explosives.

Samples	Fabrication methods	Impact sensitivity/J	Friction sensitivity	Particle sizes	Density/g·cm^{-3}	Refs
Raw RDX	–	9.0	144 N/84%	50–100 μm	1.804	99
r-RDX	Spray drying	17.1	–	1–3 μm	–	99
e_1-RDX	Spray drying	25.1	–	1–3 μm	–	99
e-RDX	Spray drying	37.6	–	1–3 μm	–	99
N-RDX	Milling, vacuum drying	14.3	58.0%	63.7 nm	–	100
G-RDX	Milling, slurry drying	11.3	78.0%	–	–	100
Nano-K-6	SASA	14.7	–	60 nm	–	44
Micro-K-6	SASA	12.3	–	–	–	44
α_e-RDX	Electrospray	10	>360 N	200–600 nm	1.819	101
α_p-RDX	Plasma-made	5	>360 N	400–900 nm	1.780	101
RDX-1	SDAS method with 3% PVA	11.8	62%	–	–	102
RDX-2	Spring drying with 3% PVA	8.2	74%	–	–	102
Raw HMX	–	5	252 N/86%	150 μm	1.895	103
γ_s-HMX (spherical)	Electrospray	10	>360 N	200–500 nm	1.837	101
γ_d-HMX (donut)	Electrospray	30	>360 N	1 μm	1.896	101
HMX	Solvent/antisolvent	–	–	–	1.895	16
nano-HMX	USASA	11.6	–	81.4 nm	–	93
O-HMX	wet milling	11.9	72%	1.2 μm	–	86
F-HMX	wet milling	15.4	58%	160 nm	–	86
s-HMX	wet milling	26.5	80%	600 nm	–	104
n-HMX	Solvent/antisolvent	8.4	82%	3.0 μm	–	104
p-HMX	riddling	22.3	32%	3.3 μm	–	104
HMX-1	SA	25.6	36%	380–580 nm	–	105
HMX-2	SA	8.5	86%	1–10 μm	–	105
HMX-3	SA	7.5	28%	10–15 μm	–	105
HMX-1	SDAS method with 3% PVA	10.9	62%	–	–	102
HMX-2	Spring drying with 3% PVA	8.0	76%	–	–	102

Note: The friction sensitivity for the explosives was tested 80 ± 1° with 2.45 MPa; the friction sensitivity was carried out at 90 °C, 3.92 MPa; SA, solvent/antisolvent method; SASA, spray assistant solvent/antisolvent method; USASA, ultrasound and spray-assisted solvent/antisolvent method; UASA, ultrasound assisted solvent/antisolvent method.

Table 3
Performance of explosives.

Samples	Fabrication methods	Impact sensitivity/J	Friction sensitivity	Particle sizes	Density/g·cm^{-3}	Refs
Raw CL-20	–	3.2	82.7 N/100%	99.5 μm	2.03	9
CL-20-1	SASA	5.5	–	15 μm	–	47
CL-20-2	SASA	6.3	–	4 μm	–	47
CL-20-3	SASA	7.8	–	1 μm	–	47
CL-20-4	SASA	10.8	–	95 nm	–	47
Ultrafine CL-20	SASA	2.2	116 N	2.31 μm	–	66
s-CL-20	SA	4.7	–	14 μm	–	42
u-CL-20	USASA	8.6	–	6 μm	–	42
us-CL-20	USASA	9.3	–	470 nm	–	106
RS-CL-20	SA	8.3		71.5 μm	2.04	107
CL-20-1	SDAS method with 3% PVA	7.6	80%		–	102
CL-20-2	Spring drying with 3% PVA	5.5	92%		–	102
LLM-105	–	16.7	–	32.6 μm	–	108
Nano-LLM-105	Spray drying	19.0	–	150 nm	–	108
LLM-105-1	self-assembly	24.5	–	20 μm	–	108
LLM-105-2	SA	21.5	–	39.4 μm	–	109
LLM-105-3	UASA	16.2	–	5.8 μm	–	109
LLM-105-4	SA	20.3	–	24.3 μm	–	109
LLM-105-5	SA	13.6	–	54.9 μm	–	109
LLM-105-6	UASA	17.9	–	11.1 μm	–	109
LLM-105-7	SA	27.0	–	27.2 μm	–	109

Note: The friction sensitivity for the explosives was tested 80 ± 1° with 2.45 MPa; the friction sensitivity was carried out at 90 °C, 3.92 MPa; SA, solvent/antisolvent method; SASA, spray assistant solvent/antisolvent method; USASA, ultrasound and spray-assisted solvent/antisolvent method; UASA, ultrasound assisted solvent/antisolvent method.

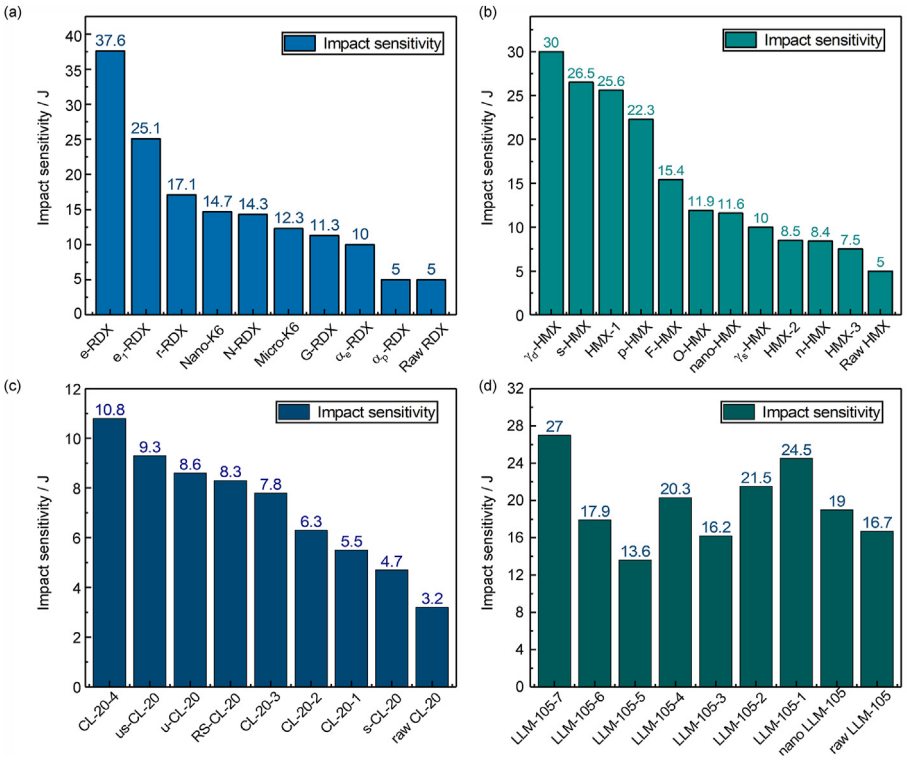

Fig. 10. The impact sensitivity of raw and crystallized RDX, HMX, CL-20 and LLM-105.

the electrospray method is best suited for HMX, as it delivers the insensitive γ_d-HMX.

Compared with raw CL-20, the average particle size, particle size distribution and crystal defects of obtained CL-20 were reduced. The rate of internal porosity of RS-CL-20 significantly decreased from 0.539 to 0.098% upon crystallization with an impact initiation energy of 8.3 J. A comparison of the impact sensitivity of different CL-20 samples, provided in Fig. 10c, reveals that the introduction of ultrasound or spray technology to the solvent/antisolvent process produced the less sensitive materials us- and s-CL-20 and that the least sensitive sample was nano-sized CL-20-4. The spray assistant solvent/antisolvent method and ultrasound (CL-20-4) and spray-assisted solvent/antisolvent method (us-CL-20) are the most suitable methods to produce insensitive CL-20 because the impact sensitivity of them are 10.8 and 9.3 J, respectively. Furthermore, the impact sensitivity decreased with the decrease in the particle size from micro-to nanometer. The impact sensitivities of HMX samples with average particle size of 15 μm, 4 μm, 1 μm, and 95 nm, prepared by solvent/antisolvent crystallization, are 5.5, 6.3, 7.3, and 10.8 J, respectively. Although nano-HMX tended to agglomerate due to the small diameter and high surface energy.

On the other hand, the sensitivity of EMs could also be increased by crystallization. As for LLM-105, the impact sensitivity of LLM-105-3 crystallized *via* ultrasound assisted solvent/antisolvent method (16.2 J) is higher than raw LLM-105 (16.7 J). The obtained LLM-105 under ultrasound has smaller particle size but with lager particle size distribution and uneven crystal morphology, which resulting in increased impact sensitivity. As the same with RDX, HMX and CL-20, the crystallization methods and conditions also affect the sensitivity of LLM-105. The impact sensitivity of nano-LLM-105 which is produced by spray drying is reduced slightly (19.0 J) while the insensitive LLM-105 with the impact sensitivity of 24.5 J could be obtained *via* self-assembled method. Moreover, the crystallization conditions like solvent and the way of dropping antisolvent have influence on sensitivity. Taking nitric acid as solvent and deionized water as antisolvent, the impact sensitivity of LLM-105-5 obtained by adding the antisolvent to solvent is just 13.6 J while the impact sensitivity of LLM-105-7 produced by adding the solvent to antisolvent is 27.0 J.

4.2. Thermal stability performance of crystallized crystals

High-quality energetic crystals, which feature a compact internal structure and few impurities or defects and are obtained by crystallization, can exhibit higher thermal stability. The thermal stability is highly influenced by crystals properties which properties could be altered by several crystallization methods. The thermal properties of several explosives obtained by crystallization are summarized in Tables 4 and 5.

The DSC curves of raw and crystallized nitramine explosives are shown in Fig. 11. The thermal stability of EMs is affected by the crystal properties such as crystal defects, particle size and purity. The thermal stability could be altered by different crystallization methods because these crystal properties could be changed by crystallization.

In general, the temperature of the endothermic peak of crystallized nitramine explosives is higher than that of raw explosives, indicating that its thermal stability improves upon crystallization. As shown in Fig. 11a, the endothermic peak of *r*-RDX obtained by spray drying and nano-RDX obtained by solvent/antisolvent crystallization are 205.6 °C and 205.5 °C while that of raw RDX is just 202.9 °C. Take HMX as an example, according to the literature, the endothermic peak of raw HMX (278.6 °C) is followed by a sharp exothermic one (284.7 °C, Fig. 11b),[103] which indicate the melting and thermal decomposition of the material, respectively. Upon crystallization, the endothermic peak is absent in all curves except for the a- and L-HMX ones (Fig. 11). Additionally, the improvement of the thermal decomposition behavior is indicated by the decrease in the lgA of the sample from 40.1 to 35.7 (Table 3).[107] The endothermic peak of CL-20 could also be reduced by crystallization which means that the some of crystallized CL-20 have higher thermal stability. As shown in Fig. 11d, heating of raw CL-20 to 160 °C triggers a solid-solid phase transition from the ϵ-to the γ-form with subsequent thermal decomposition of the latter (exothermic peak at 244.7 °C).[112] However, the endothermic peak of crystallized CL-20 *via* ultrasound and spray-assisted solvent/antisolvent method, solvent/antisolvent and spray drying method has disappeared.

On the other hand, the exothermic peaks of crystallized nitramine explosives are lower compared to raw materials except for us-CL-20 produced by ultrasound and spray-assisted solvent/antisolvent method. As shown in Table 3, the particle sizes of RDX, HMX and CL-20 have reduced after crystallization. In general, the decrease in the explosive's particle size is accompanied by the increase in the specific surface area and number of atoms on the surface. Therefore, nano-explosives exhibit larger heating surfaces and higher reaction activity. Hence, nanoparticles tend to decompose at lower temperature than larger ones.

To further explore the mechanism of decomposition, the thermal decomposition kinetic parameters of nitramine explosives are calculated using the Kissinger or Starink methods. The activation energy (E_a) of nitramine explosives decreased after crystallization. The activation energy of *r*-RDX obtained by spray drying is lower than that of raw RDX because of its smaller particle size, which facilitates heat dissipation. However, the accompanying increase in the r-RDX specific surface area leads to an apparent decrease in the activation energy. In addition, the activation energies of e− and e_1-RDX are lower than that of r-RDX because their explosive formulas contain Estane. The E_a values also are affected by crystallization methods. As for HMX, the E_a values of raw, s-HMX (wet milling), n-HMX (solvent/antisolvent), and p-HMX (ridding) are 304.3, 263.3, 241.2, and 238.2 kJ·mol^{-1}, respectively.[100] The morphology of s-, n-, and p-crystals is spherical, polyhedral, and needle-shaped, respectively. Hence, the E_a of the samples depend on the crystallization methods because the crystal morphology could be changed by crystallization. Further, the E_a values of nano- and a-HMX calculated by Kissinger method indicate that the former is more prone to thermal decomposition than micro-HMX.[109] However, the decomposition temperature and E_a of L-HMX prepared by RESS method are remarkably higher than those of the other samples.[108]

The *r*-RDX obtained by spray drying method has highest thermal stability among the crystallized RDX samples while *n*-HMX obtained by solvent/antisolvent method is the most stable crystallized HMX sample. The obtained CL-20 samples *via* ultrasound and spray-assisted solvent/antisolvent method, solvent/antisolvent and spray drying method have higher thermal stability. Thus, the solvent/antisolvent method, spray drying method are suitable to produce nitramine explosives with high thermal stability.

The thermal stability of other energetic compounds like HNS, dihydroxylammonium 5,5′-bistetrazole-1,1′-diolate (TKX-50) and LLM-105 also are affected by the crystal defects, particle size and impurity and these crystal properties could be changed by crystallization. Thus, the crystallization methods have influence on the thermal stability.[119] It shows that the temperature of exothermic peaks declines with the decrease in the particle size which is the same with nitramine explosives. For instance, the DSC curve of raw HNS (Fig. 12a) features a melt endothermic peak at 321.0 °C and an exothermic peak at 348.9 °C corresponding to thermal decomposition. In comparison, the endothermic and exothermic peaks of UF-HNS, UF-HNS-US, and UF-HNS-BM shifted to lower temperatures with the particle size of 800 nm, 470 nm and 311 nm, respectively.[120] Similarly, the exothermic peak of nano-HNS obtained by spray assistant solvent/antisolvent method has decreased by 1.1 °C compared to micro-HNS produced by solvent/antisolvent method, which is attributed to the smallest particle size and narrow size distribution. These properties result in a higher rate of energy transfer, causing the crystals to melt and decompose at lower temperatures.

The relationship between the material's properties (crystal structure and defects) and its thermal stability was studied using high-quality LLM-105-H, acid-treated LLM-105-HA, smooth spherical LLM-105-SS, and rough spherical LLM-105-SR crystals obtained by SA crystallization.[115] As shown in Fig. 12c, samples LLM-105-H and LLM-105-HA are thermally more stable than raw LLM-105. Moreover, the exothermic peaks of LLM-105-H and LLM-105-SS are located at slightly higher temperatures than those of LLM-105-HA and LLM-105-SR, respectively. Thus, the smoother surface of crystallized LLM-105 is associated with a higher thermal stability. However, the crystals with a smooth surface interact less strongly with the polymer binder, resulting in poor moldability and safety performance.

The thermal stability also can be affected by the crystallization conditions like the solvent and antisolvent. Various LLM-105 samples (a-to i-LLM-105, Table 3) were obtained by solvent/antisolvent method using water, methanol, acetic acid, nitromethane, ethyl acetate, ethanol, methylene chloride, *o*-dichlorobenzene, and toluene as the antisolvent, respectively.[73] The study revealed that the crystal habits significantly affect the thermal properties. As shown in Fig. 12, the first stage of the exothermic decomposition process occurs within a broad temperature range (252.1–325.0 °C) whereas the second occurs within a narrow range (325.0–366.7 °C). As clearly displayed, the first exothermic peak of the crystallized LLM-105 samples strongly depends on their crystal habits, with the lowest and highest values corresponding to the X-shaped crystals

Table 4
The thermal performances of explosives.

Samples	Fabrication method	E_a/kJ·mol^{-1}	lg$A$/s^{-1}	T_{P1}/°C	T_{P2}/°C	Particle size	Reference
Raw RDX	–	201.3	20.4	202.9	244.3	50–100 μm	9
r-RDX	Spray drying	205.2	21.3	205.6	242.5	1–3 μm	99
e_1-RDX	Spray drying	170.8	17.7	202.6	240.4	1–3 μm	99
e-RDX	Spray drying	190.5	19.1	205.0	241.6	1–3 μm	99
Nano-K-6	SASA	–	–	–	187.0	60 nm	44
Micro-K-6	SASA	–	–	–	195.0	–	44
Nano-RDX	SA	–	–	205.5	230.7	–	105
Raw-HMX	–	425.9	40.1	278.6	284.7	85.9 μm	103
Nano-HMX	USASA	375.4	35.7	–	279.1	81.4 nm	93
s-HMX	wet milling	263.3	–	–	285.1	600 nm	104
n-HMX	SA	238.2	–	–	284.0	3.0 μm	104
p-HMX	riddling	241.2	–	–	283.4	3.3 μm	104
L-HMX	RESS	429.4	–	552.9	557.8	76.7 μm	65
a-HMX	SA	401.6	–	279.1	282.6	5–40 μm	110
Raw CL-20	–	173.1	17.1	171.0	244.7	40 μm	70
Micro-CL-20	Wet milling	–	–	156.0	235.5	500 nm	70
Nano-CL-20	Wet milling	–	–	151.4	232.9	260 nm	70
Ultrafine CL-20	SASA	–	–	180.0	233.8	–	66
us-CL-20	USASA	173.2	17.2	–	247.3	470 nm	96
ε-CL-20	SA	198.7	18.2	–	245.2	–	111
s-CL-20	Spray drying	186.4	37.9	–	240.7	–	112
Raw HNS	–	–	–	321.0	343.5	90 μm	113
UF-HNS	SA	–	–	319.3	341.3	800 nm	113
UF-HNS-US	Ultrasound	–	–	319.4	340.9	470 nm	113
UF-HNS-BM	Wet milling	–	–	319.0	334.4	311 nm	113
m-HNS	SA	–	–	319.8	349.9	50 μm	114
n-HNS	SASA	208.9	–	321.8	348.8	120 nm	114

Note: E_a, activation energy; T_{p1}, endothermic peak; T_{p2}, exothermal peak; SA, solvent/antisolvent method; SASA, spray assistant solvent/antisolvent method; USASA, ultrasound and spray-assisted solvent/antisolvent method; UASA, ultrasound assisted solvent/antisolvent method.

Table 5
The thermal performances of explosives.

Samples	Fabrication method	E_a/kJ·mol^{-1}	lg$A$/s^{-1}	T_{P1}/°C	T_{P2}/°C	Particle size	Reference
Raw LLM-105	–	–	–	–	357.3	83.4 μm	115
LLM-105-H	SA	–	–	–	359.5	74.7 μm	115
LLM-105-HA	SA	–	–	–	358.8	71.4 μm	115
LLM-105-SS	SA	–	–	–	356.9	55.8 μm	115
LLM-105-SR	SA	–	–	–	356.3	58.7 μm	115
a-LLM-105	SA	–	–	–	347.9	–	74
b-LLM-105	SA	–	–	–	355.2	–	74
c-LLM-105	SA	–	–	–	351.0	–	74
d-LLM-105	SA	–	–	–	356.3	–	74
e-LLM-105	SA	–	–	–	353.8	–	74
f-LLM-105	SA	–	–	–	351.8	–	74
g-LLM-105	SA	–	–	–	346.3	–	74
h-LLM-105	SA	–	–	–	357.2	–	74
i-LLM-105	SA	–	–	–	357.0	–	74
Raw-TKX-50	–	–	–	–	240.1	–	116
DMA-BTO	SA	–	–	185.6	258.3	–	116
2EDA-BTO	SA	–	–	–	261.6	–	116
NHA-BTO	SA	–	–	77.8	211.7	–	116
TKX-50-1	SA	–	–	–	245.7	–	117
TKX-50-1	SA	–	–	–	244.3	–	118

Note: E_a, activation energy; T_{p1}, endothermic peak; T_{p2}, exothermal peak; SA, solvent/antisolvent method; SASA, spray assistant solvent/antisolvent method; USASA, ultrasound and spray-assisted solvent/antisolvent method; UASA, ultrasound assisted solvent/antisolvent method.

obtained from water (a-LLM-105, 270.0 °C) and the long needle-like crystals obtained from ethyl acetate (e-LLM-105, 309.8 °C), respectively. Regarding the second exothermic decomposition stage, the highest values correspond to the dendritic crystals h- and i-LLM-105 (357.0 °C and 357.2 °C, respectively). In addition, the short and flat rod-like g-LLM-105 crystals exhibit the lowest exothermic peak value at 346.3 °C.

Although the crystal quality was generally improved by crystallization, some explosives reacted with solvents. TKX-50 is stable in several solvents, including dimethyl sulfoxide (DMSO), water, and ethyl acetate, but reacts with DMF in a wide temperature range (25–150 °C) to form dimethylammonium 5,5′-bistetrazole-1-hydroxy-10-oxygen (DMA-BTO), dimethylamine 5,5′-bistetrazole-1,1′-diolate (2DMA-BTO), and diammonium 5,5′-bistetrazole-1,1′-diolate (ABTOX).[118] The presence of internal solvent can reduce the thermal stability and detonation performance. Therefore, the appropriate choice of solvent and antisolvent is crucial. The DSC curve of raw TKX-50 exhibits two exothermic peaks with the main exothermic decomposition at 240.3 °C (Fig. 12b). The thermal stability of DMA-BTO and that of NHA-BTO are lower than that of raw TKX-50, as indicated by the endothermic peaks at 185.6 °C (DMA-BTO) and at 77.8 and 136.2 °C (NHA-BTO, not displayed). Additionally, the detonation pressure and velocity of TKX-50 and derivatives were calculated using EXPLO5 and the values of the derivatives are lower than those of the parent sample raw TKX-50. In contrast, the TKX-50-1 and TKX-50-2 crystallized by solvent/antisolvent using water as solvent have higher thermal stability with the exothermic peaks at 245.7 °C and 244.3 °C, respectively.

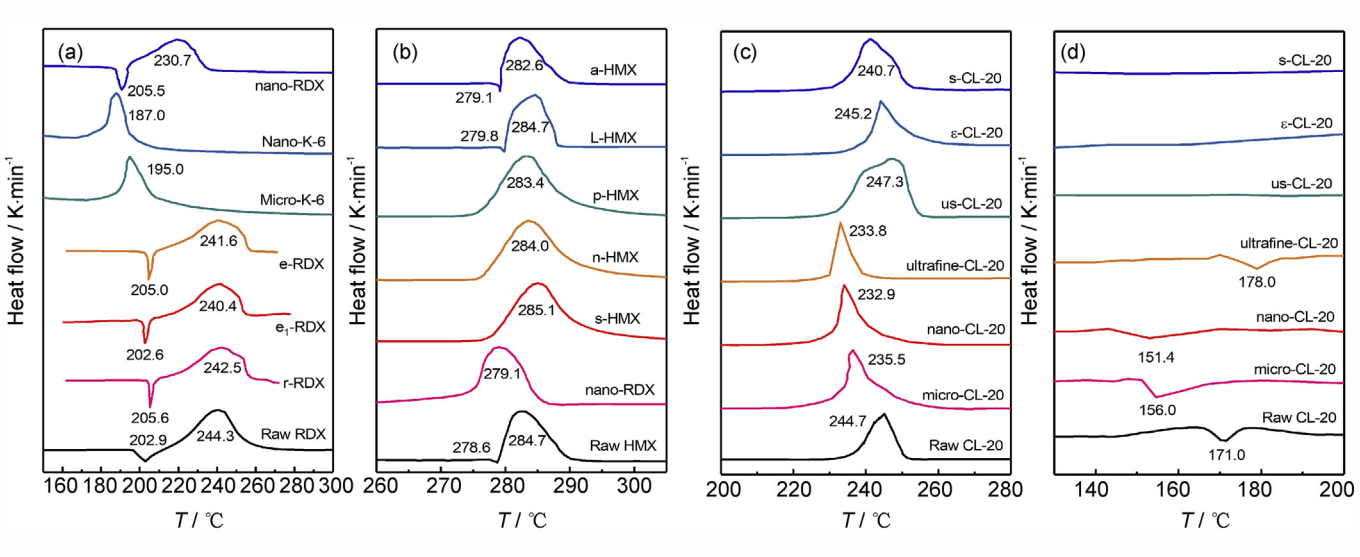

Fig. 11. DSC curves of raw and crystallized RDX, HMX and CL-20 (10 °C·min-1 heating rate).

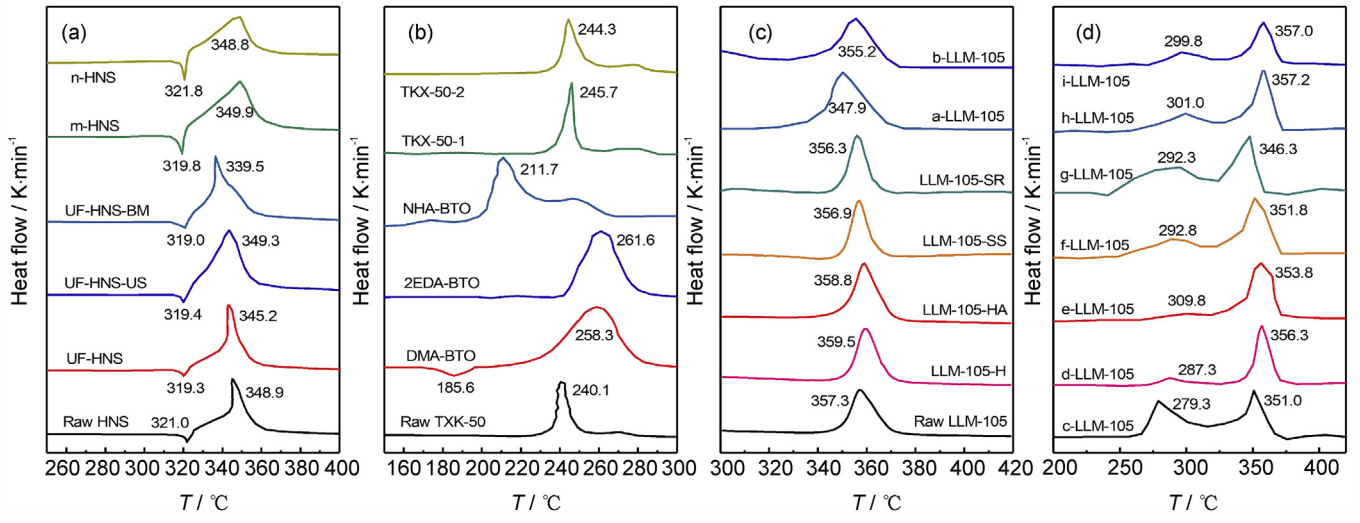

Fig. 12. DSC curves of raw and crystallized (a) HNS and (b) TKX-50 and its derivatives (10 °C·min^{-1} heating rate).

5. Concluding remarks

Crystallization is a promising strategy to balance the energy and safety of energetic crystals, by which the morphology and crystal structure can be adjusted through tuning the crystallization conditions. In particular, crystallization generally leads to a significant decrease in the crystal defects, which is reflected in the diminished probability of hot spot formation under external stimuli. Additionally, the thermal stability can be enhanced and the sensitivity decreased by this approach, as crystallized EMs generally feature smaller particle sizes and fewer inclusions and defects.

In general, energetic crystals with smaller particle sizes, fewer crystal defects, smoother surfaces, and narrower particle size distribution are less sensitive to external stimuli. The nano- and micro-sized energetic crystals were obtained by evaporation or precipitation crystallization methods. Among these, the solvent/antisolvent crystallization is the most cost-effective and commonly used one. However, it is less suited for the production of nano-sized energetic crystals with narrower particle size distribution. Thus, ultrasound- and spray-assisted techniques were introduced to solvent/antisolvent process. These techniques were also combined with other modification methods, enabling the fabrication of hybrid energetic crystals with superior structures and multi-functional properties. For example, the SDAS method is the most suitable strategy to produce high-quality RDX crystals, while defect-free spherical CL-20 crystals were obtained by the electrospray or ultrasound spray crystallization processes. In addition, the use of surfactant additives is a promising approach to prevent aggregation and access spherical crystals with a smooth surface.

As the crystallization techniques summarized herein reduce the sensitivity of distinct energetic crystals to different extents, the selection of the ideal method depends on the desired performance and available resources. Moreover, nanocrystals are less sensitive to external stimuli than the corresponding microcrystals. Overall, crystals prepared by the spray drying method exhibit high thermal stability and impact or friction energy for ignition. The HMX sample obtained by the electrospray crystallization method is the least insensitive to impact stimuli with an ignition energy of 37.6 J.

Conflicts of interest

The authors have no conflicts to declare.

Declaration of interests

The authors declare that they have no known competing financial interests or personal relationships that could have appeared to influence the work reported in this paper.

Acknowledgements

This paper was funded by NSAF project (Grant No. U2030202) and the National Defense Basic Science Foundation of China (Project No. 61407200204).

References

1. Sikder AK, Sikder N. A review of advanced high performance, insensitive and thermally stable energetic materials emerging for military and space applications. *J Hazard Mater*. 2004;112(1-2):1–15.
2. Pagoria PF, Lee GS, Mitchell AR, Schmidt RD. A review of energetic materials synthesis,. *Thermochim Acta*. 2002;384:187–204.
3. Sabatini Jesse J, Oyler Karl D. Recent advances in the synthesis of high explosive materials. *Crystals*. 2016;6(1):5.
4. Badgujar D, Talawar M, Asthana S, Mahulikar P. Advances in science and technology of modern energetic materials: an overview. *J Hazard Mater*. 2008; 151(2-3):289–305.
5. Koch E. Insensitive high explosives II: 3,3'-Diamino-4,4'-azoxyfurazan (DAAF). *Propellants, Explos Pyrotech*. 2016;41(3):526–538.
6. Xu Y, Wang Q, Shen C, Lin Q, Wang P, Lu M. A series of energetic metal pentazolate hydrates,. *Nature*. 2017;549:78–81.
7. Lin CM, Gong FY, Zhang ZJ, et al. Core-Shell structured HMX@polydopamine energetic microspheres. *Synergistically Enhanced Mechanical, Thermal, and Safety Performances*. 2019;11:568.
8. Zhu Q, Xiao C, Li SB, Luo G. Bioinspired fabrication of insensitive HMX particles with polydopamine coating. *Propellants, Explos Pyrotech*. 2016;41:1092–1097.
9. Zhang XX, He W, Chen SW, et al. Tuning the crystal morphology and catalytic behavior of graphene-templated energetic bis-tetrazole copper coordination polymers. *Adv. Compos. Hybrid Mater*. 2019;2:289–300.
10. Zhang XX, Xue ZH, Wang ZKP, Chen SW, Yang ZJ, Yan QL. Hybrid RDX crystals assembled under constraint of 2D materials with largely reduced sensitivity and improved energy density. *J Hazard Mater*. 2020;398:122842.
11. Yan QL, Yang ZJ, Zhang XX, et al. High density assembly of energetic molecules under the constraint of defected 2D materials. *J Mater Chem*. 2019;7:17806–17814.
12. Yan QL, Gozin M, Zhao F, Cohen A, Pang S. Highly energetic compositions based on functionalized carbon nanomaterials. *Nanoscale*. 2016;8(9):4799–4851.
13. Bolton O, Simke LR, Pagoria PF, Matzger AJ. High power explosive with good sensitivity: a 2:1 cocrystal of CL-20:HMX. *Cryst Growth Des*. 2012;12:4311–4314.
14. Wei C, Huang H, Duan X, Pei C. Structures and properties prediction of HMX/TATB co-crystal. *Propellants, Explos Pyrotech*. 2011;36:416–423.
15. Iohara D, Yoshida K, Yamaguchi K, et al. Cyclodextrin-Induced change in crystal habit of acetylsalicylic acid in aqueous solution. Cryst. *Growth Des*. 2012;12: 1985–1991.
16. Kröber H, Teipel U. Crystallization of insensitive HMX. *Propellants, Explos Pyrotech*. 2008;33(1):33–36.
17. Lee BM, Jeong JS, Lee YH, et al. Supercritical antisolvent micronization of cyclotrimethylenetrinitramin: influence of the organic solvent. *Ind Eng Chem Res*. 2009;48:11162–11167.
18. Pouretedal H, Damiri S, Shahsavan A. Modification of RDX and HMX crystals in procedure of solvent/anti-solvent by statistical methods of Taguchi analysis design and MLR technique. *Def. Technol*. 2018;14(1):59–63.
19. Anderson P. Crystallization. New Left review. 2013;83:13–23.
20. Vukovic M, Dinic I, Nikolic B, Marinkovic A, Costa K. Radulovic Mancic. Effects of different polymers and solvents on crystallization of the NaYF 4 :Yb/Er phase. *Bull Mater Sci*. 2020;43(1):1–10.
21. Hsien-Hsin Tung, Paul Edward L, Michael Midler, Mccauley James A. *Evaporative crystallization. In crystallization of organic compounds*. Hoboken, NJ, USA: John Wiley Sons; 2008:167–178.
22. Arpagaus C, Collenberg A, Rütti D, Assadpour E, Jafari S. Nano spray drying for encapsulation of pharmaceuticals. *Int.J.Pharm*. 2018;546(1-2):194–214.
23. Jayanthi G, Zhang S, Messing G. Modeling of solid particle formation during solution aerosol thermolysis: the evaporation stage. *Aerosol Sci Tech*. 1993;19(4): 478–490.
24. Eslamian M, Shekarriz M. Recent advances in nanoparticle preparation by spray and microemulsion methods, recent pat. *Nanotechnology*. 2009;3:99–115.
25. Wang JY, Zhang JL, Xu WZ. Experimental study on the spray-crystal ultrafine explosive HMX. *Huozhayao Xuebao/Chinese Journal of Explosives and Propellants*. 2003;26(1):33–36.
26. Fang H, Huang K, Yuan L, et al. The direct synthesis of Au nanocrystals in microdroplets using the spray-assisted method. *New J Chem*. 2016;40(9): 7294–7298.
27. Long Cheng, Chuan Huang, Yue Yang, Yifan Li, Yingyi Meng, Yanchun Li. Artiaga Ramón. Preparation and combustion performance of B/PVDF/Al composite microspheres. *Propellants, Explos Pyrotech*. 2020;45(4):657–664.
28. Radacsi N, Stankiewicz A, Van der Heijden Y, Ter Horst J Creyghton. Electrospray crystallization for high-quality submicron-sized crystals. *Chem Eng Technol*. 2011; 34(4):624–630.
29. Radacsi N, Wassink L, Stankiewicz AI, Creyghton YLM, Heijden AEDM, van der Horst JH ter, TNO Defensie en Veiligheid. *Electrospray: a simple technique to create nanosized RDX*. 2010.
30. Bartle KD, Shilstone GF, Jafar SA, Clifford AA. Solubilities of solids and liquids of low volatility in supercritical carbon dioxide. *J Phys Chem Ref Data*. 1991;20(713).
31. Turk M. formation of small organic particles by RESS: experimental and theoretical investigations. *J Supercrit Fluids*. 1999;15:79.
32. Debenedetti PG. Homogeneous nucleation in supercritical fluids. *AIChE J*. 1990;36: 1289.
33. Teipel U, Kröber H, Krause H. formation of energetic materials using supercritical fluids. *Propellants, Explos Pyrotech*. 2001;26(4):168–173.
34. Stepanov V, Krasnoperov LN, Elkina IB, Zhang X. Production of nanocrystalline RDX by rapid expansion of supercritical solutions. *Propellants, Explos Pyrotech*. 2005;30(3):178–183.
35. Byoung-Min Lee, Kim DaeSung, Lee Young-Ho, et al. Preparation of submicron-sized RDX particles by rapid expansion of solution using compressed liquid dimethyl ether. *J Supercrit Fluids*. 2011;57(3):251–258.
36. Haiyang Dou, Kim Ki-Hoon, Lee Byung-Chul, Choe Jinkyu, Kim Hyoun-Soo, Lee Seungho. Preparation and characterization of cyclo-1,3,5-trimethylene-2,4,6-trinitramine (RDX) powder: comparison of microscopy, dynamic light scattering and field-flow fractionation for size characterization. *Powder Technol*. 2013;235:814–822.
37. Afrose A, White E, Howes T, et al. Preparation of ibuprofen microparticles by antisolvent precipitation crystallization technique: characterization, formulation, and in vitro performance. *J. Pharm. Sci*. 2018;107(12):3060–3069.
38. Mersmann A. Crystallization and precipitation. *Chem Eng Process: Process Intensification*. 1999;38(4):345–353.
39. Yang GC, Nie FD, Huang H. Preparation and characterization of nano-TATB explosive. *Propellants, Explos Pyrotech*. 2006;31:390.
40. Yang G, Nie F, Huang H, Zhao L, Pang W. Preparation and characterization of nano-TATB explosive. *Propellants, Explos Pyrotech*. 2006;31(5):390–394.
41. Dalas E. The effect of ultrasonic field on calcium carbonate scale formation. *J Cryst Growth*. 2001;222(1-2):287–292.
42. Sivabalan R, Gore GM, Nair UR, Saikia A, Venugopalan S, Gandhe BR. Study on ultrasound assisted precipitation of CL-20 and its effect on morphology and sensitivity. *J Hazard Mater*. 2007;139:199.
43. Bayat Y, Eghdamtalab M, Zeynali V. Control of the particle size of submicron HMX explosive by spraying in non-solvent. *J Energetic Mater*. 2010;28(4):273–284.
44. Shokrolahi A, Zali A, Mousaviazar A, Keshavarz M, Hajhashemi H. Preparation of nano-K-6 (Nano-Keto RDX) and Determination of its characterization and thermolysis. *J Energetic Mater*. 2011;29(2):115–126.
45. Gilardi R, Flippen-Anderson JL, George C. Structures of 1,3,5-trinitro-2-oxo-1,3,5-triazacyclohexane (I) and 1,4-dinitro-2,5-dioxo-1,4-diazacyclohexane (II).Acta Crystallographica Section C. 1990;4:706–708.
46. Hu LS, Wang XJ, Gao M, Yu GS, Wang FC, Yu ZH. Mass transfer of atomization from pressure-Swirl nozzle. *J Chem Ind Eng*. 2008;59:2733 (in Chinese).
47. Bayat Y, Zeynali V. Preparation and characterization of nano-CL-20 explosive. *J Energetic Mater*. 2011;29(4):281–291.
48. Gupta S, Kumar P, Jindal D, Sharma S, Agarwal A, Lata P. Micro nozzle assisted spraying process for Re-crystallization of Submicrometer hexanitrostilbene explosive. *Propellants, Explos Pyrotech*. 2018;43(7):721–731.
49. Mayorga IC, Astilleros JM, Fernández-Díaz L. Precipitation of $CaCO_3$ polymorphs from aqueous solutions: the role of pH and sulphate groups. *Minerals*. 2019;(3):9.
50. Samsuri S, Mohd Bakri M. Optimization of fractional crystallization on crude biodiesel purification via response surface methodology. *Separ Sci Technol*. 2018;53(3):567–572.
51. Xiong G, You L, Ren B, He Y, Wang S, Sun Y. Structure and magnetocaloric effect of two kinds of Ln–MnII Heterometallic coordination polymers produced by fractional crystallization. *Eur J Inorg Chem*. 2016;2016(24):3969–3977.
52. Ulrich J, Stelzer T. Melt crystallization. In: *Crystallization: Basic Concepts and Industrial Applications*. Wiley-VCH; 2013:289–304.
53. Ponyrko S, Kobera Brus, Matějka. Epoxy-silica hybrids by nonaqueous sol–gel process. Polymer, 54(23), 6271–6282.
54. Lee Simpson, Hrubesh Tillotson. Swansiger Simpson R. Sol-gel manufactured energetic materials. *Star*. 2006;25:44.
55. Yu W, Huang H, Zhang J, et al. Nano-RDX/RF film preparation with sol-gel method. *Han Neng Cai Liao*. 2008;16(4):391–394.
56. Tian T, Zhixin Z, Vulpe D, Casco m E, Divitini G, midgley PA, Fairen-Jimenez D. A sol–gel monolithic metal–organic framework with enhanced methane uptake. *Nat Mater*. 2017;17(2):174–179.
57. Jia XL. Fabrication and characterization of submicron-sized RDX with reduced sensitivity via green mechanical demulsification technology. *Huozhayao Xuebao/Chinese Journal of Explosives and Propellants*. 2019;42(6):571–576.
58. Spitzer D, Comet M, Baras C, Pichot V, Piazzon N. Energetic nano-materials: Opportunities for enhanced performances. *J Phys Chem Solid*. 2010;71:100–108.
59. Roberts C, Hira S, Mason B, Strouse G, Stoltz C. Controlling RDX explosive crystallite morphology and inclusion content via simple ultrasonic agitation and solvent evaporation. *CrystEngComm*. 2011;13(4):1074–1076.

60. Moore J. Barnes Izvekov, Lísal Sellers, Taylor Brennan. A coarse-grain force field for RDX: density dependent and energy conserving. *J Chem Phys*. 2016;144(10):104501.
61. Chen F, Zhou T, Wang M. Spheroidal crystal morphology of RDX in mixed solvent systems predicted by molecular dynamics. *J Phys Chem Solid*. 2020:136.
62. Czerski H. Greenaway proud field. Links between the morphology of RDX crystals and their shock sensitivity. *AIP Conference Proceedings*. 2006;845(1):1053–1056.
63. Qiu H, Stepanov V, Di Stasio A, Surapaneni A, Lee W. Investigation of the crystallization of RDX during spray drying. *Powder Technol*. 2015;274:333–337.
64. Chen G, Xia M, Lei W, Wang F, Gong X. A study of the solvent effect on the morphology of RDX crystal by molecular modeling method. *J Mol Model*. 2013;19(12):5397–5406.
65. Soo-Jung K, Byoung-min L, Byung-Chul L, Hyoun-Soo K, Hwayong K, Youn-Woo L. Recrystallization of cyclotetramethylenetetranitramine (HMX) using gas anti-solvent (GAS) process. *J Supercrit Fluids*. 2011;59:108–116.
66. Gupta S, Kumar P, Sharma S, Kaur G, Agarwal A, Lata P. Pressurized nozzle-based solvent/AntiSolvent process for making ultrafine ε-CL-20 explosive. *Propellants, Explos Pyrotech*. 2017;42(7):773–783.
67. Erofeev LN, Tarasov YP, Kalmykov YB. Crystal defects and stability of RDX. *Russ Chem Bull*. 2001;50(6):1000–1002.
68. Bouma R, Van der Heijden A. The effect of RDX crystal defect structure on mechanical response of a polymer-Bonded explosive. *Propellants, Explos Pyrotech*. 2016;41(3):484–493.
69. Kumar R, Soni P, Siril P. Engineering the morphology and particle size of high energetic compounds using drop-by-drop and drop-to-drop solvent-antisolvent interaction methods. *ACS Omega*. 2019;4(3):5424–5433.
70. Wang D, Gao B, Yang G, Nie F, Huang H. Preparation of CL-20 explosive nanoparticles and their thermal decomposition property. *J Nanomater*. 2016:1–7.
71. Mrinal Ghosh, Shaibal B, Shafeeuulla K, Abdul Md, Nirmala S, Kanti SA. Understanding metastable phase transformation during crystallization of RDX, HMX and CL-20: experimental and DFT studies. *Phys Chem Chem Phys*. 2016; 18(34):23554–23571.
72. Lovette MA, Doherty MF. Needle-Shaped Crystals: Causality and Solvent Selection Guidance based on periodic bond Chains. Cryst. *Growth Des*. 2013;13:3341–3352.
73. Zhou X, Zhang Q, Xu R, et al. A novel Spherulitic self-assembly strategy for organic explosives: modifying the hydrogen bonds by polymeric additives in emulsion crystallization. *Cryst Growth Des*. 2018;18(4):2417–2423.
74. Zhou X, Chen D, Li H, Shan J. Tuning the crystal habits of organic explosives by antisolvent crystallization: the case study of 2,6-dimaino-3,5-dinitropyrazine-1-oxid (LLM-105). *Crystals*. 2019;9(8).
75. Duan X, Liu C, Qiao Y, et al. Dendrite growth of energetic material RDX. *J Cryst Growth*. 2012;351(1):56–61.
76. Achuthan CP, Jose CI. Studies on octahydro-1,3,5,7-tetranitro-1,3,5,7-tetrazocine (HMX) polymorphism. *Propellants, Explos Pyrotech*. 1990;15:271–275.
77. Cady HH, Larson AC, Cromer DT. Crystal structure of a HMX and a refinement of the structure of b-HMX. *Acta Crystallogr*. 1963;16:617–623.
78. Mrinal G, Banerjee S, Khan S, Sikder MdAbdul, Sikder Nirmala, Kanti Arun. Understanding metastable phase transformation during crystallization of RDX, HMX and CL-20: experimental and DFT studies. *Phys Chem Chem Phys*. 2016; 18(34):23554–23571, 2016.
79. Millar D, MaynardCasely H, Kleppe A, Marshall W, Pulham C, Cumming A. Putting the Squeeze on energetic materials structural Characterisation of A high-pressure phase of CL-20. *CrystEngComm*. 2010;12:2524–2527.
80. Foltz MF, Coon CL, Garcia F, Nichols AL. The thermal stability of the polymorphs of hexanitrohexaazaisowurtzitane, Part I. *Propellants, Explos Pyrotech*. 1994;19:19–25.
81. Nair UR, Sivabalan R, Gore GM, Geetha M, Asthana SN, Singh H. Hexanitrohexaazaisowurtzitane (CL-20) and CL-20based formulations. *Combust Explos Shock Waves*. 2005;41:121–132.
82. Pelikán V, Zeman S, Yan Q, Erben M, Elbeih A, Akstein Z. Concerning the shock sensitivity of cyclic nitramines incorporated into a polyisobutylene matrix. *Cent. Eur. J. Energ. Mater*. 2014;11:219–235.
83. Foltz MF, Coon CL, Garcia F, Nichols AL. The thermal ttability of the polymorphs of hexanitrohexaazaisowurtzitane,. *Part II. Propell Explos Pyrot*. 1994;19:133–144.
84. Xu J, Tian Y, Liu Y, Zhang H, Shu Y, Sun J. Polymorphism in hexanitrohexaazaisowurtzitane crystallized from solution. *J Cryst Growth*. 2012; 354(1):13–19.
85. Zhang YX, Liu DB, Lv CX. Preparation and characterization of Reticular nano-HMX. *Propellants, Explos Pyrotech*. 2005;30:438.
86. Liu YC, Wang JH. CW. An Effect of particle size of RDX on mechanical sensitivity. *Chin J Explos Propellants*. 2004;27:7–9.
87. Siviour CR, Gifford MJ, Walley SM, Proud WG, Field JE. Particle size effects on the mechanical properties of a polymer bonded explosive. *J Mater Sci*. 2004;39:1255–1258.
88. Stepanov V, Krasnoperov L, Elkina I, Zhang X. Production of nanocrystalline RDX by rapid expansion of supercritical solutions. *Propellants, Explos Pyrotech*. 2005; 30(3):178–183.
89. Jun-Woo Kim, moon-Soo Shin, Jae-Kyeong Kim, Hyoun-Soo Kim, Kee-Kahb Koo. Evaporation crystallization of RDX by ultrasonic spray. *Ind Eng Chem Res*. 2011; 50(21):12186–12193.
90. An C, Li H, Guo W, Geng X, Wang J. Nano Cyclotetramethylene tetranitramine particles prepared by a green recrystallization process. *Propellants, Explos Pyrotech*. 2014;39(5):701–706.
91. Xu WZ, Pang ZY, Wang J, Ping C. Ultrafine high quality HMX prepared by ultrasonic assisted spray method and its crystal type control. *Hanneng Cailiao/ Chinese Journal of Energetic Materials*. 2018;26(3):260–266.
92. Suh W, Suslick K. Magnetic and porous nanospheres from ultrasonic spray pyrolysis. *J Am Chem Soc*. 2005;127(34):12007–12010.
93. Jie Liu, Wei Jiang, Fengsheng Li, Longxiang Wang, Jiangbao Zeng, Qing Li, Wang Yi, qing Yang. Effect of drying conditions on the particle size, dispersion state, and mechanical sensitivities of nano HMX. *Propellants, Explos Pyrotech*. 2014;39(1):30–39.
94. Talawar MB, Sivabalan T, mukundan H, muthurajan AK, Sikder BR, Gandhe Rao AS. environmentally compatible next generation green energetic materials (GEMs). *J Hazard Mater*. 2009;161:589–607.
95. Zhang C, Jiao F, Li H. Crystal engineering for creating low sensitivity and highly energetic materials. *Cryst Growth Des*. 2018;18:5713–5726.
96. Pivkina A, Ulyanova P, Frolov Y. Nanomaterials for heterogeneous combustion. *Propellants, Explos Pyrotech*. 2004;29:39–48.
97. Qiu H, Stepanov V, Di Stasio A, Chou T, Lee W. RDX-based nanocomposite microparticles for significantly reduced shock sensitivity. *J Hazard Mater*. 2011; 185(1):489–493.
98. Joshi KaushikL, Chaudhuri Santanu. Reactive simulation of the chemistry behind the condensed-phase ignition of RDX from hot spots. *Phys Chem Chem Phys*. 2015; 17:18790–18801.
99. Yan XD, Li XF, Zhou P, Shi X, Ji W. Preparation of insensitive RDX by suspension spray technology and its characterization. *Cent Eur J Energ Mat*. 2019;16(2):216–227.
100. Jie Liu, Longxiang Wang, Qing Li, Jiangbao Zeng, Sai Zhou, Jiang Wei, Fengsheng Li. Preparation and characterization of insensitive nano RDX. *Chin J Explos Propellants*. 2012;35(6):46–50.
101. Norbert Radacsi, Bouma RichardHB, Krabbendam-laaHaye Ellen LM, TeraHorst Joop H, Stankiewicz AndrzejI, VanaderaHeijden Antoine EDM. On the Reliability of sensitivity test methods for Submicrometer-sized RDX and HMX particles. *Propellants, Explos Pyrotech*. 2013;38(6):761.
102. Jia X, Wei L, Liu X, et al. Fabrication and characterization of submicron scale spherical RDX, HMX, and CL-20 without soft agglomeration. *J Nanomater*. 2019:8.
103. Zhang XN, Xu GG, Xu JP, Wang WM. A study about impact sensitivity of ultrafine HMX and HMX,. *Chin J Explos Propellants*. 1999;22:33–36.
104. Song XL, Wang Y, An CW, Guo XD, Li FS. Dependence of particle morphology and size on the mechanical sensitivity and thermal stability of octahydro-1,3,5,7-tetranitro-1,3,5,7tetrazocine. *J Hazard Mater*. 2008;159(222).
105. Kumar R, Siril P, Soni P. Preparation of nano-RDX by evaporation assisted solvent-antisolvent interaction. *Propellants, Explos Pyrotech*. 2014;39(3):383–389.
106. Jingyu Wang, Li Junlong, An Chongwei, Hou Conghua, Xu Wenzheng, Li Xiaodong. Study on ultrasound- and spray-assisted precipitation of CL-20. *Propellants, Explos Pyrotech*. 2012;37(6):670–675.
107. Hong-Zhen Li, Rong Xu, Ming Huang, Fu-De Nie, Jian-Hua Zhou, Hui Huang. Preparation and properties of reduced-sensitivity CL-20. *Chin J Energetic Mater*. 2009;17(1):125.
108. Yang Z, Gong F, He G, et al. Perfect energetic crystals with improved performances obtained by thermally metastable interfacial self-assembly of corresponding nanocrystals. *Cryst Growth Des*. 2018;18:1657–1665.
109. Rong Xu, Yu-Liao Long, Wang Cun-Shu, Zhang Yong. Influence of Recrystallizatjon method on crystal properties and performance of LLM-105. *Acta Armamentarii*. 2015;11:2099–2103.
110. Shijie Zhang, Gao Zhenguo, Jia Qian, Liu Ning, Zhang Jiaoqiang, Kou Kaichang. Fabrication and characterization of surface modified HMX@PANI core-shell composites with enhanced thermal properties and desensitization via in situ polymerization. *Appl Surf Sci*. 2020:515.
111. Zhang JY, Guo XY, Jiao QJ, Zhang HL, Li H. Analysis of the thermal behaviour of CL-20, potassium perchlorate, lithium perchlorate and their Admixtures by DSC and TG. *Cent Eur J Energ Mat*. 2018;15(1):115–130.
112. Xu WZ, Peng JY, Wang J, Li H, Wang JY. Preparation and characterization of CL-20 based composites by compressed air spray evaporation, cent. *Eur. J. Energ. Mater*. 2020;17:66–84.
113. Pandita P, Arya VP, Kaur G, et al. Size reduction of HNS to Nanoscale by in tandem application of Chemo-mechanical methods. *Propellants, Explos Pyrotech*. 2019;44(3): 301–312.
114. Wang Jingyu, Huang Hao, Xu WenZheng, et al. Prefilming twin-fluid nozzle assisted precipitation method for preparing nanocrystalline HNS and its characterization. *J Hazard Mater*. 2009;162(2-3):842–847.
115. Yang Z, Lin C, Gong F, Zeng C, Zhang J, Huang F. Effects of crystal quality and morphology on the mechanical performance of LLM-105 based PBXs. *Propellants, Explos Pyrotech*. 2019;44(10):1219–1225.
116. Xin Xu, Chen Dong, Li Hongzhen, et al. Crystal structure evolution of an energetic compound dihydroxylammonium 5,5-bistetrazole-1,1-diolate induced by solvents. *RSC Adv*. 2020;10(20):11939–11944.
117. Huang H, Shi Y, Yang J. Thermal characterization of the promising energetic material TKX-50. *J Therm Anal Calorim*. 2015;121(2):705–709.
118. Jia J, Liu Y, Huang S, et al. Crystal structure transformation and step-by-step thermal decomposition behavior of dihydroxylammonium 5,5-bistetrazole-1,1-diolate. *RSC Adv*. 2017;7(77):49105–49113.
119. Bari R, Koh Y, Mckenna G, Simon S. Decomposition of HMX in solid and liquid states under nanoconfinement. *Thermochimica*. 2020:686.
120. Yang Z, Gong F, He G, et al. Perfect energetic crystals with improved performances obtained by thermally metastable interfacial self-assembly of corresponding nanocrystals. *Cryst Growth Des*. 2018;18:1657–1665.

Xue-Xue Zhang is a master student in the academic committee of the national Key Laboratory on Combustion and Explosion, Northwestern Polytechnical University (NPU). She mainly focuses on the functional materials which can improve the combustion performance of solid propellants. In addition, she is doing researches on reducing the sensitivity of energetic oxidizer and turning the combustion performance of solid propellants. She has published 3 papers as the first author.

Qi-Long Yan is a Full Professor in the Northwestern Polytechnical University (NPU). He is a member of the academic committee of the national Key Laboratory on Combustion and Explosion, focusing his research on preparation, characterization, and reactivity of nanocomposite energetic materials. Before joining in NPU, he was a Postdoctoral Fellow at the Center of Nanoscience and Nanotechnology, Tel Aviv University (Israel). He obtained his Ph.D. in 2015 from the University of Pardubice (Czech Republic). He is currently serving as an adjunct professor for Institution of chemical materials, CAEP (China). He is also on the editorial boards of several journals including Chin J Propellants Explos, Energetic Mater Frontier and Chin J Energet Mater. He is authored with over 120 papers, two books, and 11 patents.